Carbohydrate Polymers 227 (2020) 115339

Contents lists available at ScienceDirect

Carbohydrate Polymers

journal homepage: www.elsevier.com/locate/carbpol

# Reconstructed chitosan with alkylamine for enhanced gene delivery by promoting endosomal escape

Guojun Huang[a,b], Qi Chen[a,b], Wangteng Wu[a,c], Jianwei Wang[a], Paul K. Chu[b], Hongzhen Bai[a,*], Guping Tang[a,b,*]

[a] Department of Chemistry, Zhejiang University, Hangzhou 310028, China
[b] Department of Physics and Department of Materials Science and Engineering, City University of Hong Kong, Tat Chee Avenue, Kowloon, Hong Kong, China
[c] School of Medicine, Zhejiang University, Hangzhou 310019, China

ARTICLE INFO

*Keywords:*
Alkylamine
Chitosan
Buffering capacity
Endosomal escape
Gene delivery

ABSTRACT

Poor buffering capacity of chitosan (CS) results in insufficient intracellular gene release which poses the major barrier in gene delivery. Herein, we reconstructed pristine CS with propylamine (PA), (diethylamino) propylamine (DEAPA), and *N, N*-dimethyl- dipropylenetriamine (DMAMAPA) to obtain a series of alkylamine-chitosan (AA-CS). The introduction of multiple amino groups with rational ratios functionally enhance the buffering capacity of AA-CS, among which DMAPAPA-CS showed buffering capacity of 1.58 times that of chitosan. The reconstructed AA-CS functionally enhance the ability of gene binding and endosomal escape. It was observed that the DMAPAPA-CS/pDNA complexes exhibit a notable gene delivery efficiency, which promotes the functionalization of loaded pDNA. Importantly, the *in vivo* delivery assay reveals that the deep penetration issue can be resolved using DMAPAPA-CS gene delivery vector. Finally, the DMAPAPA-CS is applied to deliver the therapeutic p53 gene in A549 bearing mice, showing efficient therapeutic potential for cancer.

## 1. Introduction

Gene delivery is a genetic therapeutic strategy to treat inheritable or gene disorder-associated diseases by silencing pathogenic genes, transporting therapeutic gene, or substituting missing genes in specific tissues or cells (Nielsen, 1998; Verma & Somia, 1997; Li et al., 2011; Jiang et al., 2011; Wu et al., 2017). Development of the appropriate nanocarrier is one of critical steps of gene delivery. As the only natural positive polysaccharide, chitosan has been proposed as an applicable gene carrier because of its cationic characteristic and biocompatibility (Byeon, Kim, Thompson, & Roberts, 2014; Rudzinski & Aminabhavi, 2010; Yang, Gao, Dagnaes-Hansen, Jakobsen, & Kjems, 2017; Han, Tang, & Yin, 2015; Martins et al., 2019). Despite the promising advantages, the chitosan-based gene delivery system suffers from the low transfection efficiency limited by the extracellular and intracellular barriers, particularly the poor buffering capacity (Li et al., 2011; Liu et al., 2007; Ragelle, Vandermeulen, & Préat, 2013). It is a critical step that the nucleic acid-chitosan complexes escaping from the endosome and releasing the nucleic acid into cytoplasm. Based on the proton sponge mechanism, when the nucleic acid-cationic polymer complexes enter the cells, they are surrounded by the endosomal membrane. With endosomal pH changing, the cationic polymer becomes protonated, causing diffusion of water into the endosome. Eventually, the osmotic pressure is sufficient to disrupt the membrane resulting in escape of nucleic acid into the cytoplasm. Unfortunately, chitosan possesses a comparatively weak endo-lysosomalytic proton sponge effect due to the low buffering capacity, resulting in a low transfection performance (Kim, Kim, Akaike, & Cho, 2005; Lai & Wong, 2018; Ragelle et al., 2013). Strategies has been developed toward chitosan for more efficient endosomal escape (Mao, Sun, & Kissel, 2010). Poly (propyl acrylic acid) (PPAA) has been incorporated into chitosan-DNA nanoparticles to enhance gene expression. Since the pH-sensitive polymer PPAA exhibits maximum endosomal membrane disruption ability, it can facilitate the gene release into cytoplasm (Kiang et al., 2004). Poly(ethylenimine) (PEI) has been grafted onto chitosan to form PEI-g-chitosan. This gene carrier exhibits dramatically enhanced transfection efficiency. The high transfection is believed to arise from the proton sponge effect of PEI (Jiang, Kim et al., 2007; Nam & Nah, 2016; Bao et al., 2014; Boussif et al., 1995; Sonawane, Szoka, & Verkman, 2003). However, in spite of recent progress, the buffering capacity of most of the modified chitosan has not been evaluated systematically, and the link between chemical modification and function optimization is not well understood.

In this work, a series of reconstructed chitosan polycations with alkylamines were designed to optimize the properties of chitosan,

* Corresponding authors at: Department of Chemistry, Zhejiang University, Hangzhou 310028, China.
*E-mail addresses:* hongzhen_bai@zju.edu.cn (H. Bai), tangguping@zju.edu.cn (G. Tang).

https://doi.org/10.1016/j.carbpol.2019.115339
Received 7 May 2019; Received in revised form 7 September 2019; Accepted 15 September 2019
Available online 19 September 2019

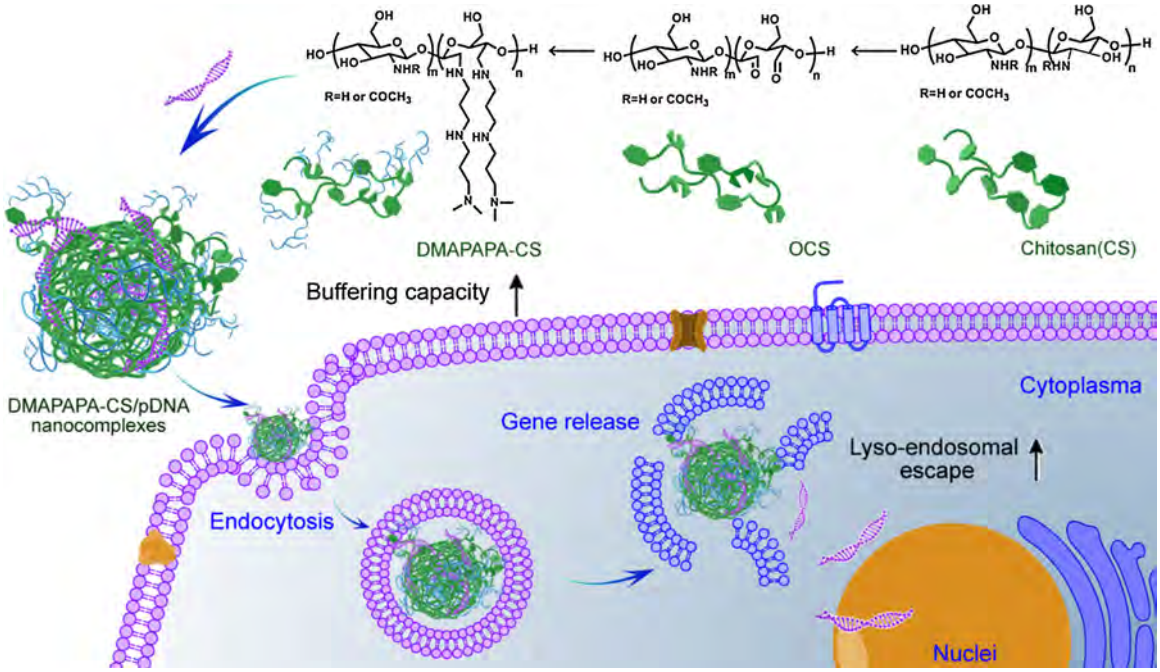


**Scheme 1.** Schematic illustration of synthesis of AA-CS and electrostatically interacted with gene to form complexes. DMAPAPA-CS/gene for effective intracellular gene delivery as efficient endosomal escape.

particularly, the buffering capacity. Different from general modification on amino groups in chitosan, we adapted a synthetic route by cyclo-opening of glucosamine units with periodate oxidized reaction, followed by reductive amination with propylamine (PA), (diethylamino) propylamine (DEAPA), and *N, N*-dimethyldipropylenetriamine (DMAPAPA) (Scheme 1). The grafted alkylamines rearranged the primary, secondary, and tertiary amines of chitosan matrix. The AA-CS polycations exhibited excellent biocompatibility inherited from chitosan. Simultaneously, they possessed an improved nucleic acid binding capacity. We also systematically evaluated the buffering capacity of AA-CS by acid-base titration in endosomal condition. Owing to the multiple amino groups, AA-CS had higher buffering capacities than chitosan, and the highest was achieved by DMAPAPA-CS. In comparison, DMAPAPA-CS displayed superior cell internalization and endosomal escape, and manifested an enhanced transfection efficiency. By verifying in A549 tumor cells, we demonstrated that DMAPAPA-CS could efficiently transport the therapeutic plasmid p53 into A549 cells. With plasmid functionalization, apoptosis was induced in A549 cells at high level. *In vivo* studies on A549 tumor-bearing mice showed that DMAPAPA-CS/p53 could permeate into tumor tissue, and significantly inhibited the tumor progression. Taken together, the DMAPAPA-CS overcomes the deficiency of chitosan on endosomal escape, posing a potential platform for gene therapy.

## 2. Experimental part

### 2.1. Materials and chemicals

Chitosan ($M_W$: 100–300 kDa, degree of deacetylation ≥ 90%) was purchased from J&K Chemical Ltd. (Shanghai) and chitosan oligosaccharide ($M_W$: 5 kDa, degree of deacetylation ≥ 85%) was provide by Yuhuan Marine Biochemistry Co., Ltd. (Yunhuan, China). Sodium periodate ($NaIO_4$, 99%), ethylene glycol, sodium cyanoboro hydride ($NaBH_3CN$, ≥ 95%), propylamine (PA, 99%), (diethylamino) propylamine (DEAPA, 99%), *N, N*-dimethyldipropylenetriamine (DMAPAPA, 99%), PEI (branched, Mw: 600 & 25 kDa, 98%), chlorpromazine (CPZ), methyl-β-cyclodextrin (MCD), amiloride (AMI), nystatin (NYS) and fluorescamine (98%) were obtained from Sigmae-Aldrich (St. Louis, MO, USA). All chemicals were reagent grade and used without further purification.

3-(4, 5-dimethylthiazol-2-yl)-2, 5-diphenyltetrazolium bromide (MTT) (Taizhou, Zhejiang, China), Trypsin-EDTA, and fetal bovine serum (FBS) were obtained from Gibco-BRL (Burlington, Canada). The Dulbecco's modified eagle medium (DMEM) medium, RPMI 1640 medium, and penicillin-streptomycin were purchased from Bristol-Myers Squibb Trading Co. Ltd. (Shanghai, China). Lyso tracker Green was bought from the Thermo Fisher Scientific-CN (Shanghai), and nuclease-free water was supplied by Sangon Biotech (Shanghai, China). The dialysis membranes were purchased from Spectrum Labs (Rancho Dominguez, USA), GFP plasmid, p53 plasmid, fluorescein-tagged negative-control siRNA (FAM-siRNA, Cy5-siRNA), and siRNA targeting green fluorescent protein (siGFP) was purchased from Keygen Biotech (Nanjing, Jiangsu, China), Rhodamine-labeled pDNA (pDNA-rho) was prepared according to the manufacturer's protocol (Label IT® Nucleic Acid Labeling Kits).

### 2.2. Cells and animals

The cell lines used in this study were purchased from ATCC. The human embryonic kidney cells HEK293 were cultured in Dulbecco's Modified Eagle's Medium (DMEM) supplemented with 10% calf serum (FCS). The human lung carcinoma cells A549 were cultured in RPMI 1640 culture medium supplemented with 10% FCS, the human breast adenocarcinoma cell line MCF-7 were cultured in RPMI 1640 culture medium supplemented with 10% FBS. The cells were cultured at 37 °C in a humidified atmosphere containing 5% $CO_2$.

BALB/c female nude mice (6–8 weeks old, 16–18 g) were purchased from the Zhejiang Chinese Medical University and maintained in a pathogen-free environment under controlled humidity and temperature. The animal experiments were performed in accordance with the China Animal Protection Law (CAPN) and the protocols were approved by the Zhejiang University Animal Care and Use Committee.

### 2.3. Synthesis of alkylamine-chitosan

#### 2.3.1. Periodate oxidation of chitosan

Periodate oxidized chitosan was prepared by a modified method of Vold and Christensen (2005); Sirvio, Hyvakko, Liimatainen, Niinimaki, and Hormi, 2011). Briefly, 5 g of chitosan were dissolved in the sodium acetate buffer (pH 4.0) at a concentration of 1.5% w/w and sodium periodate with a final concentration of 75 mM was added slowly. The reaction proceeded at room temperature under vigorous stirring for 4 h without light. Thereafter, 1.4 mL (25 mmol) of ethylene glycol were added and stirred for another 1 h to eliminate unreacted periodate. The oxidized polymer was dialyzed in a cellulose membrane tube (molecular weight cut off 7 kDa) against flowing demineralized water for 3 days. Finally, the product oxidized chitosan (OCS) was freeze dried for two days under reduced pressure and stored at low temperature.

#### 2.3.2. Reductive amination of OCS

Reductive amination of OCS was performed using a modified method of Müller, Rahmat, Sarti, Leithner, and Bernkop-Schnürch, 2012). In brief, a 10-fold excess of the amine compounds (PA, DEAPA, DMAPA, and PEI600) in relation to aldehyde groups of OCS was mixed with deionized water and the pH was adjusted to 5.0 with HCl. The mixture was incubated for 24 h under stirring at room temperature. Afterwards, the pH of solution was adjusted to neutral, and ten equivalent of sodium cyanoboro hydride to amines was added and the solution was stirred for an additional 48 h. The reduced polymer was isolated by exhaustive dialysis against demineralized water with 2 mM HCl for 12 h, 24 h against 2 mM HCl containing 1% sodium chloride (NaCl), 12 h again against 2 mM HCl, and finally against demineralized water at 10 °C in darkness for 24 h, the dialysis medium was changed every 4 h. The purified AA-CS was lyophilized and stored under the conditions described above.

### 2.4. Characterization of polymers

The $^1$H NMR spectra of the chemicals were used to verify the chemical structures. $^1$H NMR (400 MHz) was conducted on a Bruker DRX-400 spectrometer (Bruker, Ettlingen, Germany). The molecular weight (Mw) of AA-CS were carried out by gel permeation chromatography (GPC) using a PL aquagel-OH MIXED-H column (Agilent, United States) with 0.2 M $CH_3COOH/CH_3COONa$ buffer as an eluent with flow rate of 1.0 mL/min (commercially available chitosan oligosaccharide was used for calibration).The particle size and zeta potential of the micelles were determined by dynamic light scattering (DLS) on the Zetasizer 3000 (Malvern Instrument, Worcestershire, UK) at 25 °C. The fluorescence measurements were carried out on the Shimadzu RF-6000 spectrofluorophotometer. The elemental analysis were performed on the Vario MICRO cube (Elementar Analysen systeme, Germany).

### 2.5. Fluorescamine assay

The degrees of the aldehyde groups of OCS and amino group ratio of AA-CS (PA-CS, DEAPA-CS and DMAPAPA-CS) were determined by quantification of the free amino groups on chitosan using the fluorescamine assay. 100 μL of the test solution (0.5 mg/mL) and 100 μL of the fluorescamine solution (0.5 mg/mL in acetonitrile) were added to 5 mL of a 100 mM boric acid buffer solution (pH = 8). After incubation for 10 min at room temperature, fluorescence from the solution was monitored on a spectrofluorophotometer at the excitation wavelength of 392 nm and emission wavelength of 478 nm. The boric acid assay buffer was used to determine the background of fluorescence.

With regard to the degree of aldehyde groups of OCS, the mass fraction of the chitosan monomer (CSm) in the OCS solution (m%(CSm)) was calculated by the fluorescence intensity of the OCS solution as well as chitosan fluorescamine assay standard curve. The mol fraction of aldehyde-chitosan (mol%(CS-CHO)) was calculated by Eq. (1):

$$\text{mol\%(CS}-\text{CHO)} = \frac{\frac{1\times(1-\text{m\% (CSm)})}{\text{Mw(CS}-\text{CHO)}}}{\frac{1\times(1-\text{m\% (CSm)})}{\text{Mw(CS}-\text{CHO)}} + \frac{1\times\text{m\% (CSm)}}{\text{Mw(CSm)}}} \times 100\% \quad (1)$$

Similarly, the mol fraction of the Amine-Chitosan monomer (mol%(AA-CSm)) was calculated as follows. The nitrogenous mass fractions of chitosan and AA-CS (mol%(N, CS) and mol%(N, AA-CS)) were determined by elemental analysis (Elementar Analysen systeme, Germany) and the mass fraction of CSm in AA-CS (m%(CSm)) was calculated by the fluorescence intensity of the AA-CS solution and chitosan fluorescamine assay standard curve. The nitrogen mass fraction of the AA-CS monomer (AA-CSm) (m%(N, AA-CSm)) was calculated using the chemical formula and the mole fraction of AA-CS (mol%(AA-CSm)) was calculated by Eqs. (2 and 3):

$$\text{m\%(AA}-\text{CSm)} = \frac{\text{m\%(N,AA}-\text{CS)} - [\text{m\%(CSm)}\times\text{m\%(N, CS)}]}{\text{m\%(N,AA}-\text{CSm)}} \times 100\% \quad (2)$$

$$\text{mol\%(AA}-\text{CSm)} = \frac{\frac{1\times\text{m\% (AA}-\text{CSm)}}{\text{Mw(AA}-\text{CSm)}}}{\frac{1\times\text{m\% (AA}-\text{CSm)}}{\text{Mw(AA}-\text{CSm)}} + \frac{1\times\text{m\% (CSm)}}{\text{Mw(CSm)}}} \times 100\% \quad (3)$$

The percentage of amino group in AA-CS was calculated according m%(CSm) and average value of mol%(AA-CSm).

### 2.6. Buffering capacities of polycations

The proton buffering capacities of polyctions AA-CS were measured by traditional acid-base titration (Shen et al., 2013). 6 mg of polycation were dissolved in 30 mL of 0.15 M NaCl and the initial pH was changed to 3.0 with 0.1 M HCl. The basic polycation solution was adjusted to a pH of 10.0 with 0.025 M sodium hydroxide (NaOH) as monitored by a microprocessor pH meter (Hanna Instruments PH211, Ann Arbor, MI) after addition of each aliquot. Chitosan (5 kDa) served as the control.

### 2.7. Preparation of complexes

The AA-CS/gene complex was prepared by manual mixing. Accurately weighed AA-CS was dissolved in nuclease-free water (Sangon Biotech, Shanghai) and the pDNA or siRNA was diluted to a working concentration of 0.1 mg/mL before complexation. AA-CS/gene with the desired weight ratios was formed by simple electrostatic complexation followed by addition of the AA-CS solution with an equal volume. The complexes were vortexed gently and kept at room temperature for 0.5 h before use.

### 2.8. Gel retardation assay

To prepare the agarose gels, agarose (1.0 mg, Sigma-Aldrich) was dissolved in the warm TRIS acetate-EDTA (TAE) buffer solution (1 ×, 100 mL) and after cooling, the nucleic acid gel stain Gel Red 10,000 × stock reagent (diluted into the molten agarose gel solution at 1:10,000) was pipetted into the solution and mixed thoroughly. The solution was poured into the gel tray. Combs were carefully placed and used to remove any bubbles for covering and to harden. The DMAPAPA-CS/DNA complexes were loaded onto the agarose gel by mixing with the loading buffer. Gel electrophoresis was carried out in the 1 × TAE buffer at 80 V for 30 min on a Sub-Cell system (Bio-rad Laboratories, CA). The gel analyzed with a UV illuminator showed the position of the complexed DNA relative to the naked DNA.

### 2.9. DNase protection assay

Protection of DNA from DNase was performed by a modified method of DNase I protection assay (Richardson, Kolbe, & Duncan,

1999; Sahoo, Banerjee, Ghosh, & Chattopadhyay, 2014). Briefly, the naked plasmid DNA (1 μg) or polyplexes were prepared to a final volume of 20 μL and the solution were divided into two tubes. 2 μL of DNase I (2 units) or phosphate buffer saline (PBS) in the DNase/$Mg^{2+}$ digestion buffer (50 mM, Tris–Cl, pH 7.6 and 10 mM $MgCl_2$) were added to each tube. The samples were incubated at 37 °C under shaking at 100 rpm for 45 min. After incubation, the samples were treated with 5 μL of EDTA (100 Mm) for 10 min to inactivate the DNase. Finally, 10 μL of 5 mg/mL heparin were added to each tube and incubated for 2 h at room temperature to allow complete dissociation of the complexes. Gel electrophoresis was carried out in 1 × TAE buffer at 80 V and 200 mA for 30 min on a Sub-Cell system (Biorad Laboratories, CA).

### 2.10. In vitro transfection assay

Prior to transfection, the HEK293 cells were seeded onto 24-well plates at a density of $4 \times 10^4$ cells/well. After cultivation at 37 °C for 16 h. The cell medium was aspirated and the cells were rinsed with PBS before exposure to 400 μL fresh serum-free 1640 containing complexes with 1 μg pDNA in different weight ratios for full binding. Lipofectamine™ 2000 Transfection Reagent (Invitrogen) was applied to the cells according to manufacturer's protocols as the control. After incubation for 4 h at 37 °C, the transfection medium was replaced with the fresh growth medium and the cells were incubated for another 48 h.

The luciferase activity was determined according to standard protocols of the luciferase assay system (Promega). The measurements were conducted in a single-tube luminometer (Berthold lumat LB9507, Germany) for 10 s. The relative light units (RLU) were normalized against the protein concentration in the cell extracts measured using the BCA protein assay kit (Pierce, Rockford, USA). The luciferase expression efficiency was reported in terms of RLU/mg cellular protein.

### 2.11. Cellular uptake

The cellular uptake and distribution were examined by confocal microscopy. $5 \times 10^4$ per well A549 cells were seeded onto 24-well plates and grew for 24 h. 1 μg of pDNA or siRNA was complexed with AA-CS at a suitable weight ratio at room temperature for 30 min before use. After cell uptake for periods, the cell nuclei were counterstained with Hoechst 33342 (blue fluorescence) and lysosome was stained with Lyso Tracker Green. The images were acquired under a confocal scanning laser microscope (CLSM, Olympus IX81-FV1000).

Internalization of complexes was analyzed by flow cytometry (Beckman-Cytoflex, USA). Formation of the complexes and delivery to cells were completed as described above and chitosan/pDNA was the control. The mean fluorescence intensity (MFI) increase of pDNA internalization was compared to the control.

### 2.12. Determination of endocytosis pathways

The endocytosis pathways were determined according to the method of Q. Hu et al. (2015). A549 cells ($1 \times 10^5$ cells per well) were seeded in the 6-well plates and cultured for 24 h. In order to investigate the endocytosis pathway, the cells were pre-incubated with various kinds of endocytosis inhibitor, including clathrin-mediated endocytosis: chlorpromazine (CPZ, 10 μM); inhibitor of caveolin-mediated endocytosis: nystatin (NYS, 25 μg/mL); inhibitor of micropinocytosis: amiloride (AMI, 1 mM); inhibitor of lipid raft: methyl-β-cyclodextrin (MCD, 3 mM) for 1 h at 37 °C, respectively. Afterwards, the cells were incubated with AA-CS/pDNA in the presence of inhibitors for additional 4 h. After washing the cells with PBS twice, the fluorescence intensity of cells were measured via flow cytometry

### 2.13. Cell viability and live-dead assay

The MTT method was used to evaluate the cell viability. Prior to exposure to the polycation solutions, the cells were seeded into a 96-well plate. After cultivation for 16 h, the cells were incubated with various concentrations of AA-CS solutions at 37 °C for 24 h. 5 mg/mL MTT solution was added to the 96-well plate and the mixture was incubated for 4 h. The formazan crystals were dissolved in 100 μL of DMSO per well and measured on a microplate reader (Model 680, Bio-Rad) at a wavelength of 570 nm. The untreated cells served as the 100% cell viability control and the completely dead cells served as the blank. The relative cell viability (%) related to control cells was calculated using the following formula: $V\% = ([A]_{experimental} - [A]_{blank})/([A]_{control} - [A]_{blank}) \times 100\%$, where $V\%$ is the cell viability (%), $[A]_{experimental}$ is the absorbance of the wells containing the treated cells, $[A]_{blank}$ is the absorbance of the blank, and $[A]_{control}$ is the absorbance of the wells containing the untreated cells.

Determination of live and dead cells. The A549 cells were incubation with AA-CS solutions for 24 h. After staining with calcein-AM and PI, an Olympus IX71 biological inverted microscope (Japan) was used to observe the viable and dead cells.

### 2.14. Hemolysis

The blood compatibility of AA-CS was evaluated by hemolysis tests on mouse red blood cells (RBC) according to the method of Liu et al. (2016). In brief, the anti-coagulated blood was diluted with PBS and centrifuged at 1500 rpm for 10 min at 4 °C. The erythrocyte pellets on the bottom of centrifuge tube were collected and washed three times with PBS. The RBC suspension was diluted with PBS to produce a stock RBC solution. 0.5 mL of the RBC stock solution were incubated with different concentrations of AA-CS and the volume was adjusted to 1.0 mL with PBS. RBCs after incubation with water and PBS were used as the positive and negative controls, respectively. The resulting mixtures were incubated at 37 °C for 4 h and centrifuged at 1500 rpm at 4 °C for 10 min. The absorbance of the supernatant solution of the test sample ($A_{test}$), positive control ($A_{pos}$), and negative control ($A_{neg}$) at 540 nm was determined by UV–vis spectrophotometry. Each set of experiments was carried out three times and the hemolysis (%) = $[(A_{test} - A_{neg})/(A_{pos} - A_{neg})] \times 100\%$.

### 2.15. Western blot

Western blotting analysis was used in the analysis of the expression of p53 protein in A549 cell lines. The cell proteins were extracted after different treatments and the total protein was quantified by the BCA protein assay kit (Promega, USA). An equal amount of protein was separated on the SDS-PAGE, transferred onto the nitro-cellulose membrane, blocked, and incubated overnight with monoclonal antibodies against p53 and GADPH. After washing, the membrane was incubated with the horseradish peroxidase-conjugated secondary antibody for 2 h at room temperature. The bands were visualized using the Westzol enhanced chemiluminescence kit (Intron, Sungnam, Korea) and the expression was normalized to the housekeeping gene expression.

### 2.16. Cell apoptosis analyses

A total of $1 \times 10^5$ A549 cells per well were seeded in 6-well plates and transfected with CS/p53, PA-CS/p53, DEAPA-CS/p53, and DMAPAPA-CS/p53, respectively. CS/p53 plasmid was used as control, PEI-CS/p53 was used as a positive gene delivery control. To detect cell apoptosis, A549 cells were collected at 72 h after transfection and apoptosis was measured by using an Annexin V-FITC/PI Apoptosis Detection Kit (Invitrogen) with flow cytometry (Beckman-Cytoflex, USA).

### 2.17. Biodistribution and tumor inhibition in vivo

The animal experiments were performed in accordance with the

regulations of China Animal Protection Network and all the protocols in the study were approved by the Zhejiang University Animal Care and Use Committee. BALB/c female nude mice (5–6 weeks, 15–18 g weight) were purchased from Zhejiang University Animal Care Center and maintained in a pathogen-free environment at a controlled temperature of 25 °C. The A549 cells were transplanted into the left or right abdominal of the mice to establish the tumor models.

Tumor orthotopic injection was performed using the modified method of Shi et al. (2003). To investigate the biodistribution of the AA-CS/siRNA complex in the tumor tissue, the female BALB/c nude mice bearing lung tumors were randomly assigned to four groups with the tumor orthotopic injected with 100 μL of 5% glucose solution containing 2 μg of FAM-siRNA complexed with PA-CS, DEAPA-CS, DMAPAPA-CS and PEI-CS, respectively. At 3 h after administration, the mice were sacrificed and tumors were collected and sectioned into slides. The photographs were taken with a digital camera attached to the inverted fluorescence microscope (IFM).

To evaluate the anticancer effects of the DMAPAPA-CS/p53 gene delivery system *in vivo*, we first established A549 xenograft in 6-week-old female BALB/c nude mice. In details, $1 \times 10^7$ A549 cells were inoculated subcutaneously into fossa axillaries of 12 nude mice (n = 3 per group). PBS, naked p53 plasmid, CS/p53 or DMAPAPA-CS/p53 (20 μg of p53 plasmid per mice) were peritumoral injected subcutaneously into xenografts. Tumor volumes and body weight were measured every 3 days after tumor volumes equaled to or were greater than 50 $mm^3$. At day 21, the mice were killed, and their tumors were immediately harvested and weighted.

## 3. Results and discussion

### 3.1. Synthesis and characterization of alkylamine-chitosan

Chitosan with Mw of 100–300 kDa (D.D. ≥ 85%) was employed as the matrix for synthesis of the alkylamine-chitosan (AA-CS) (Scheme 1). The periodate oxidation was conducted to prepare the oxidized chitosan (OCS). The C—C bond of 1, 2-amino alcohols of chitosan was cleaved by periodate ions forming the dialdehyde-chitosan. The vicinal diols, 1,2-hydroxy ketones, 1,2-diketones, α-keto acids, α-hydroxy acids, amino acids, 1,2-diamines, epoxides, and, 1,2-dioxygenated groups were also oxidatively cleaved by periodate, but the acetylation groups in the chitosan were not affected during the reaction (Jiang, Kwon et al., 2007; Vold & Christensen, 2005). The OCS was analyzed by $^1$H NMR the proton peak of the 2-carbon of chitosan decreased due to the cleavage of C—C bond. By comparing the integral values of the proton peak assigned to 2-carbon (Fig. 1B-C), the degree of dialdehyde-chitosan was determined from 16 mol% to 54 mol%. The fluorescamine assay was performed by the standard curve (Fig. S1) and the results were listed in Table S1, confirming the degree of dialdehyde-chitosan (Corsi, Chellat, Yahia, & Fernandes, 2003; Schroedter & Weller, 2002).

Fourier transform infrared (FTIR) spectra were shown in Fig. 1E. For chitosan, the characteristic absorption band at 3416 $cm^{-1}$ was related to the stretching vibration of N—H and O—H bonds. The stretching vibration of C–H bonds was located at 2930 $cm^{-1}$. The absorption peaks at 1630 $cm^{-1}$, 1518 $cm^{-1}$, and 1381 $cm^{-1}$ were assigned to the stretching amide carbonyl (C═O), N—H angular deformation, and $CH_3$ symmetrical angular deformation bonds, respectively. Characteristic peaks at 1155 $cm^{-1}$ and 1077 $cm^{-1}$ were related to C—O stretching of the β(1→4) glycoside bonds (Edson, Ingato, Wu, Lee, & Kwon, 2018; Rahimi, Safa, & Salehi, 2017). After periodate oxidation, the peak of the carbonyl group in chitosan at 1630 $cm^{-1}$ shifted to 1650 $cm^{-1}$, which was attributed to the coexist of carbonyl group and newly formed aldehyde group (enol). The larger integral of the peak at 1050 $cm^{-1}$, stretching vibration of C—O bond, verified the formation of enol. The partially cleaved OCS provided reactive sites on the chitosan backbone, allowing further reactions with alkylamines.

The OCS with a degree of 30% dialdehyde-chitosan was reconstructed by grafting with alkylamines including PA, DEAPA, DMAPAPA (Fig. 1A). After reductive amination with alkylamines, AA-CS was confirmed by $^1$H NMR (Fig. S2-S4 and Fig. 1D). In $^1$H NMR spectrum of DMAPAPA-CS (Fig. S4), chemical shifts at 4.6 ~ 3.3 ppm were assigned to the proton peaks of chitosan backbone. The peaks at 3.3 ~ 1.5 ppm indicated that DMAPAPA was conjugated onto the chitosan. PEI-CS was also synthesized and served as a reference polymer. The $^1$H NMR spectrum of PEI-CS was shown in Fig. S5.

The ratio of conjugated amine groups in AA-CS were determined by $^1$H NMR, fluorescamine assay and elemental analysis (Fig. 1F). The results indicated that the nitrogenous mass fractions of chitosan, PA-CS, DEAPA-CS, and DMAPAPA-CS were 7.43 ± 0.16%, 7.11 ± 0.04%, 6.89 ± 0.08%, and 8.47 ± 0.07%, respectively. The decreasing of primary amine groups on PA-CS, DEAPA-CS and DMAPAPA-CS were quantified by the fluorescamine assay (Fig. 1G). The results suggested that the primary amine groups of chitosan were substituted by secondary and tertiary amine groups of PA, DEAPA, and DMAPAPA. The ratios of multiple amine groups on PA-CS, DEAPA-CS, and DMAPAPA-CS were calculated by Eqs. (2) and (3). Approximately, 20 mol% of alkylamines were conjugated to the chitosan backbone (Table S2) and the ratios of multiple amine groups were listed in Fig. 1H. The ratio of primary to secondary to tertiary amine groups of DMAPAPA-CS was estimated at 56.9: 28.7: 14.4, and the ratio of PEI-CS was 45.8: 36.1: 18.1. The evidence suggested the successful reconstruction of cleaved chitosan by introducing a series of alkylamines to different degrees. The molecular weight of AA-CS were determined by GPC. The Mn (number average molecular weight), Mw (weight average molecular weight) and Mw/Mn (the polydispersity) of AA-CS were listed in Table S3, the Mws of the AA-CS were range from 8.0 to 9.7 kDa.

### 3.2. Buffering capacity of AA-CS

Multiple amino groups with rational ratios would functionally enhance the buffering capacity. AA-CS rearranged the primary, secondary, and tertiary amines, and the theoretical assignment of multiple amines was shown in Fig. 1H. To evaluate the proton buffering capacities of AA-CS, the acid-base titration was conducted in pH from 4.0 to 10.0, PEI-CS and PEI-25 kDa were set as control (Fig. 2A and S6). The sudden changes were correspond to the peak in the first-order derivative of the titration curve (Fig. 2B). The peak was caused by the buffering action of AA-CS in the pH range between 6.5 and 9.0. The buffering capacities (β, β = db/dpH) of DMAPAPA-CS, PEI-CS and PEI-25 kDa were 0.27 ± 0.05, 0.28 ± 0.01, and 0.33 ± 0.05 respectively, 1.6 ~ 1.9 times higher than that of chitosan (0.17 ± 0.04). The β values of PA-CS and DEAPA-CS were similar to that of chitosan, 0.12 ± 0.04 and 0.14 ± 0.01, respectively (Fig. 2C). It could be concluded that DMAPAPA-CS and PEI-CS had higher proton buffering capacities at pH 6.5 ~ 9.0, which was attributed to their rational assignments of multiple amines.

### 3.3. Biocompatibility of alkylamine-chitosan

In order to evaluate the biocompatibility of AA-CS, the cytotoxicity and blood compatibility were assessed in the dosage of 0 - 200 μg/mL. The cytotoxicity of AA-CS was determined by MTT assay upon A549 (Fig. 3A), MCF-7 and HEK293 (Fig. S7) cell lines. PA-CS, DEAPA-CS, and DMAPAPA-CS showed barely detectable cytotoxicity for the three cell lines after incubation for 24 h. The cell viability was over 80%, slightly decreasing in a dose-dependent manner. PEI-CS exhibited higher cytotoxicity (about 62.33% in A549 cells line at 200 μg/mL), which was reported to be attributed to the grafted PEI. PEI (25 kDa) showed high cytotoxicity in HEK 293, MCF-7 and A549 cells. Concerning the blood compatibility of AA-CS, the hemolysis assay was conducted with the concentration up to 500 μg/mL (Fig. 3B). AA-CS induced extremely few hemolytic effects (hemolysis percentage < 2%) after cocultivation with red blood cells (RBCs) for 4 h at 37 °C. The RBCs

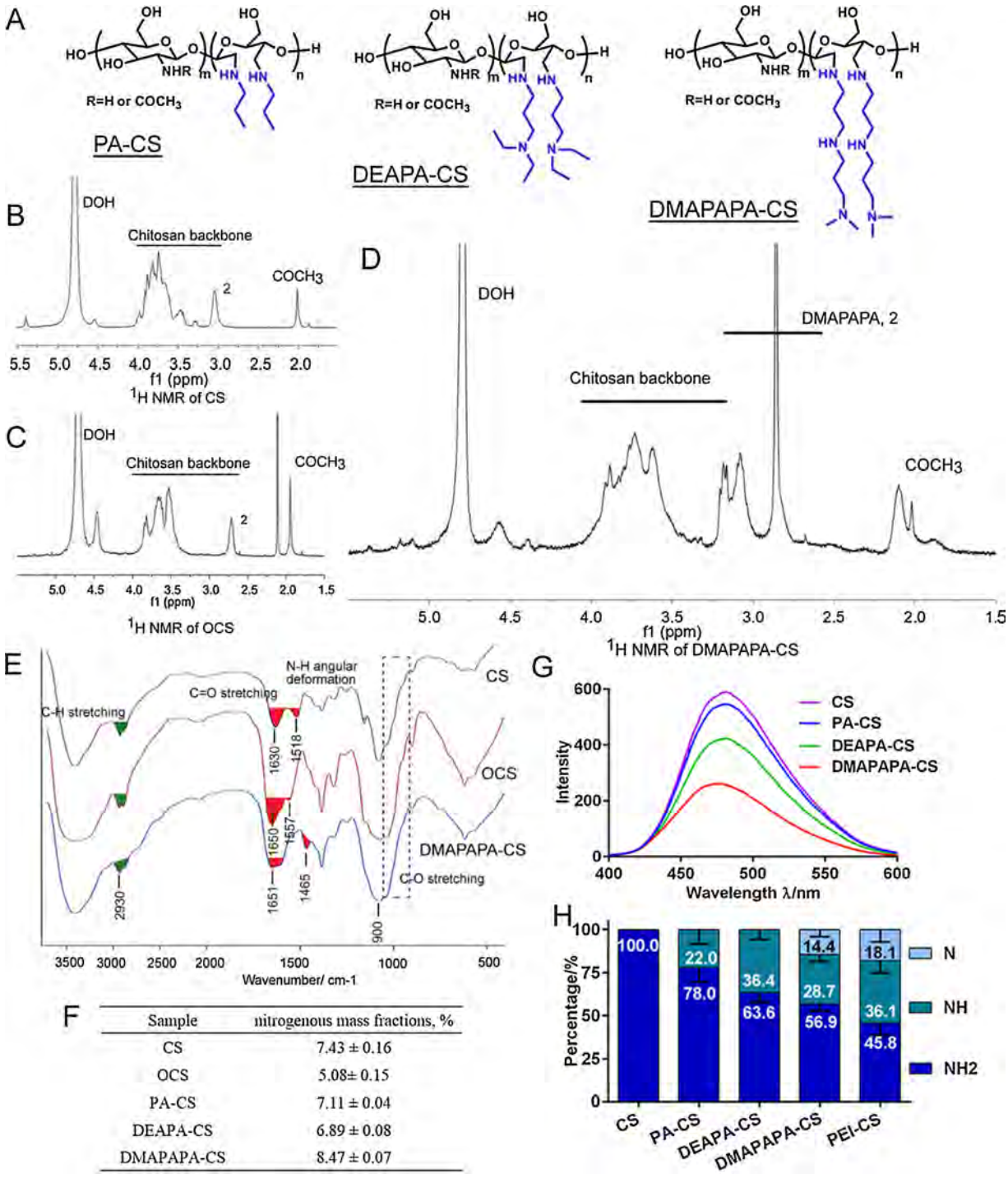


F

| Sample | nitrogenous mass fractions, % |
|---|---|
| CS | 7.43 ± 0.16 |
| OCS | 5.08± 0.15 |
| PA-CS | 7.11 ± 0.04 |
| DEAPA-CS | 6.89 ± 0.08 |
| DMAPAPA-CS | 8.47 ± 0.07 |

**Fig. 1.** Synthesis and characterization of alkylamine-chitosan: (**A**) Reconstructed AA-CS including PA-CS, DEAPA-CS, and DMAPAPA-CS; $^{1}$H NMR spectra of (**B**) CS, (**C**) OCS, and (**D**) DMAPAPA-CS in $D_2O$; (**E**) Fourier transform infrared (FTIR) spectra of CS, OCS, and DMAPAPA-CS, respectively; (**F**) Elemental analysis of CS, OCS, and AA-CS; (**G**) Fluorescent spectra of CS and AA-CS after reacting with fluorescamine; (**H**) Ratios of multiple amine groups on chitosan and AA-CS based on the Elemental analysis, $^{1}$H NMR and fluorescamine assay.

treated with water or PEI (25 kDa) showed a red color, exhibiting obvious hemolytic effects. By contrast, AA-CS solutions were still clear (Fig. 3B and S8). The live-dead staining was carried out in cells treated with AA-CS (Fig. 3C), confirming the low cytotoxicity of AA-CS. The results implied that AA-CS would not induce cytotoxicity or hemolysis within a reasonable dosage range, showing a potential for biological applications.

### *3.4. Preparation and physicochemical characterization of AA-CS/gene complexes*

To verify the pDNA binding ability of AA-CS, the retardation of AA-CS/pDNA complexes in the agarose gel was assessed by electrophoretic mobility shift assay (EMSA) with different weight ratios. By adding the AA-CS solution to DNA with equal volumes, the AA-CS/pDNA complexes were formed by electrostatic complexation (Fig. 3D). As shown in Fig. 3E, the PA-CS, DEAPA-CS, DMAPAPA-CS, and PEI-CS (as positive

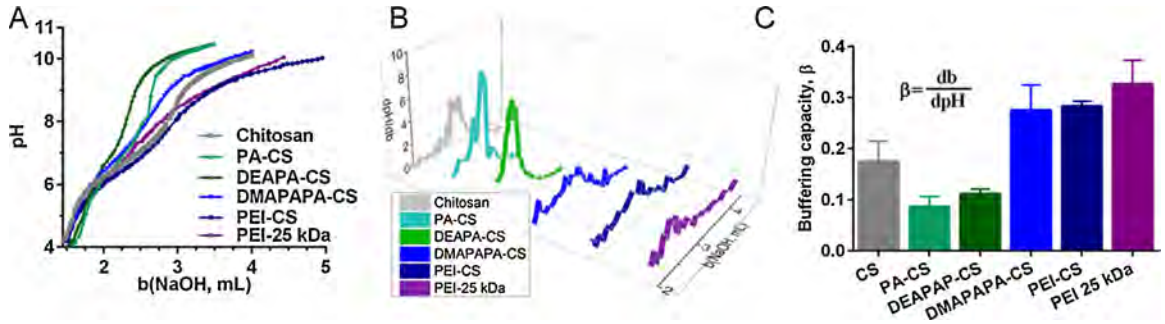


**Fig. 2.** Buffering capacity of AA-CS: (**A**) Acid-base titration profiles of AA-CS; (**B**) First-order derivative (dpH/db) of the titration curve of AA-CS; (**C**) db/dpH of the peak in the first-order derivative curve.

control) could completely retard migration of pDNA in the agarose gel at weight ratios (w/w) of 40, 20, 3.0 and 2.0, respectively. In comparison with chitosan, AA-CS, especially DMAPAPA-CS, exhibited a superior pDNA affinity. The high affinity of DMAPAPA-CS and PEI-CS was derived from the enhanced interaction provided by the additional secondary and tertiary amines. Moreover, topological reconstruction of chitosan facilitated pDNA encapsulating. The flexible alkylamines served as molecular brushes or pseudopods to sterically tangle with pDNA, stabilizing the AA-CS/pDNA complexes. The particle size and zeta potential were monitored upon AA-CS/pDNA complexes (Fig. S9). The complexes were almost neutral with the weight ratios increasing, and their surface charge became positive. The size of AA-CS/pDNA complexes were measured by DLS, for example, the size of DMAPAPA-CS/DNA complex (weight ratio of 5/1) was 106.1 ± 23.13 nm (Fig. 3F). Similarly, the PA-CS, DEAPA-CS, DMAPAPA-CS, and PEI-CS could also completely retard migration of siRNA in the agarose gel at weight ratios (w/w) of 50, 30, 10 and 8, respectively (Fig. S10 and S11). The morphology of AA-CS/pDNA complexes was observed under TEM (Fig. 3G and S12). The complexes exhibited spherical shape with a diameter of 80–150 nm, consistent with the DLS measurement. The protective capacity of AA-CS to prevent DNA degradation from DNase I was studied by gel electrophoresis (Fig. S13). The percentage of undegraded DNA was then analyzed by ImageJ (Fig. 3H). There was about 89.4%, 93.0% and 56.04% of undegraded DNA releasing from PA-CS/pDNA, DEAPA-CS/pDNA, and DMAPAPA-CS/pDNA, respectively. The weak DNA-protecting capacity of DMAPAPA-CS was attributed to low content of DMAPAPA-CS in the complex (Fig. 3E). As that, we calculated the DNase protection ability by undegraded DNA to AA-CS cost ratio (Fig. 3I). The DMAPAPA-CS showed higher DNase protection ability, demonstrating that DMAPAPA-CS efficiently protects genes from enzymatic degradation by steric encapsulation with genes. The cytotoxicity of AA-CS/pDNA complexes was evaluated as a function of weight ratio of AA-CS/pDNA upon different cell lines (Fig. S14). The results indicated that the complexes induced little cytotoxicity, benefiting pDNA transportation and functionalization.

### 3.5. Cell uptake and endosomal escape of AA-CS

To investigate the gene transporting performance of AA-CS, the cellular uptake of AA-CS/pDNA complexes were studied by CLSM. The Rhodamine-labeled pDNA (pDNA-rho) was condensed with AA-CS to form nanoparticles and co-incubated with A549 cells for 4 h. The endocytosis of the AA-CS/pDNA complexes was monitored by CLSM (Fig. 4A). The cells treated with the PA-CS/pDNA complexes exhibited accumulations of pDNA-rho signal at cytomembrane. On the contrary, the cells incubated with the DMAPAPA-CS/pDNA complexes enabled the detection of intense accumulations in the cytoplasm, indicating an efficient cell internalization of the loaded pDNA mediated by DMAPAPA-CS. The intracellular trafficking of AA-CS/siRNA was also carried out (Fig. S15). The cellular uptake of AA-CS/siRNA complexes were also studied by flow cytometry (Fig. S16). In comparison, the DMAPAPA-CS/siRNA complexes displayed a superior cell internalization.

We next evaluated the intracellular pathways of DMAPAPA-CS/pDNA-rho by testing the relative uptake efficiencies in the A549 cells treated with various endocytosis inhibitors. The quantification by flow cytometry demonstrated that DMAPAPA-CS/pDNA-rho was internalized by cells via the clathrin-dependent endocytosis with the involvement of lipid raft (Hu et al., 2015) (Fig. 4C). The intracellular trafficking of DMAPAPA-CS/pDNA-rho complexes were then monitored by CLSM to investigate the endosomal escape. Meanwhile, PEI-CS/pDNA-rho and PEI-25 kDa/pDNA-rho complexes were employed as control groups. After a short incubation of 0.5 h, overwhelming yellow fluorescence was observed (Fig. 4B), indicating the internalized DMAPAPA-CS/pDNA-rho nanoparticles were preferentially localized in late endosomes/lysosomes. Similar phenomenon was also observed in PEI-CS/pDNA-rho and PEI-25 kDa/pDNA-rho groups. With the extension of incubation for 4 h, the red signal disseminated in cytoplasm, suggesting part of DMAPAPA-CS/pDNA-rho nanoparticles successfully escaped from late endosomes/lysosomes. In PEI-CS/pDNA-rho or PEI-25 kDa/pDNA-rho group, red signal was also diffused in cytoplasm, while the treated cells looked crumpled and irregular, presenting an unhealthy state. On the contrary, cells in DMAPAPA-CS /pDNA-rho were not impaired under the treatment. Taken together, DMAPAPA-CS displayed an efficient endosomal/lysosomal escape without inducing cytotoxicity, facilitating the release and functionalization of the loaded gene.

### 3.6. Transfection and p53 functionalization mediated by AA-CS in vitro

Encouraged by the efficient cell internalization and endosomal escape, we next investigated the transfection behavior of AA-CS polycations. Luciferase activity assay of AA-CS/pGL-4 complexes was performed upon A549, HEK293 and MCF-7 cell lines. The transfection results in relative light units (RLU)/mg protein of treated HEK293 cells demonstrated that AA-CS/pGL-4 significantly improved the transfection efficiency as compared to chitosan. Particularly, DMAPAPA-CS/pGL-4 or PEI-CS/pDNA group showed the highest RLU, the values being 2 and 3 orders of magnitudes higher than that of CS/DNA, respectively (Fig. S17A). Similar outcomes were obtained from the A549 (Fig. 4D) and MCF-7 cells (Fig. S17B). Luciferase expression in CS/pGL-4 or PA-CS/pGL-4 group was undetected (UD) for A549 cells. As to MCF-7 cells, CS/pGL-4 or PA-CS/pGL-4 complex induced only $\sim 10^3$ RLU/mg protein of luciferase expression. On the contrary, PEI-CS/pGL-4 and DMAPAPA-CS/pGL-4 complexes displayed $10^4 \sim 10^5$ RLU/mg protein and $10^5$ RLU/mg protein of luciferase expression, respectively. In addition, the GFP plasmid (pGFP) transfection mediated by AA-CS, PEI-CS, PEI 25 kDa, and Lipofectamine 2000 has been carried out in HEK293 and A549 cells (Fig. S18). The results suggested that AA-CS polycations, particularly, DMAPAPA-CS and PEI-CS, significantly enhanced transfection efficiency as compared to the pristine chitosan. Thus, the reconstructed chitosan with alkylamines proposed a significant strategy to overcome the transfection barrier.

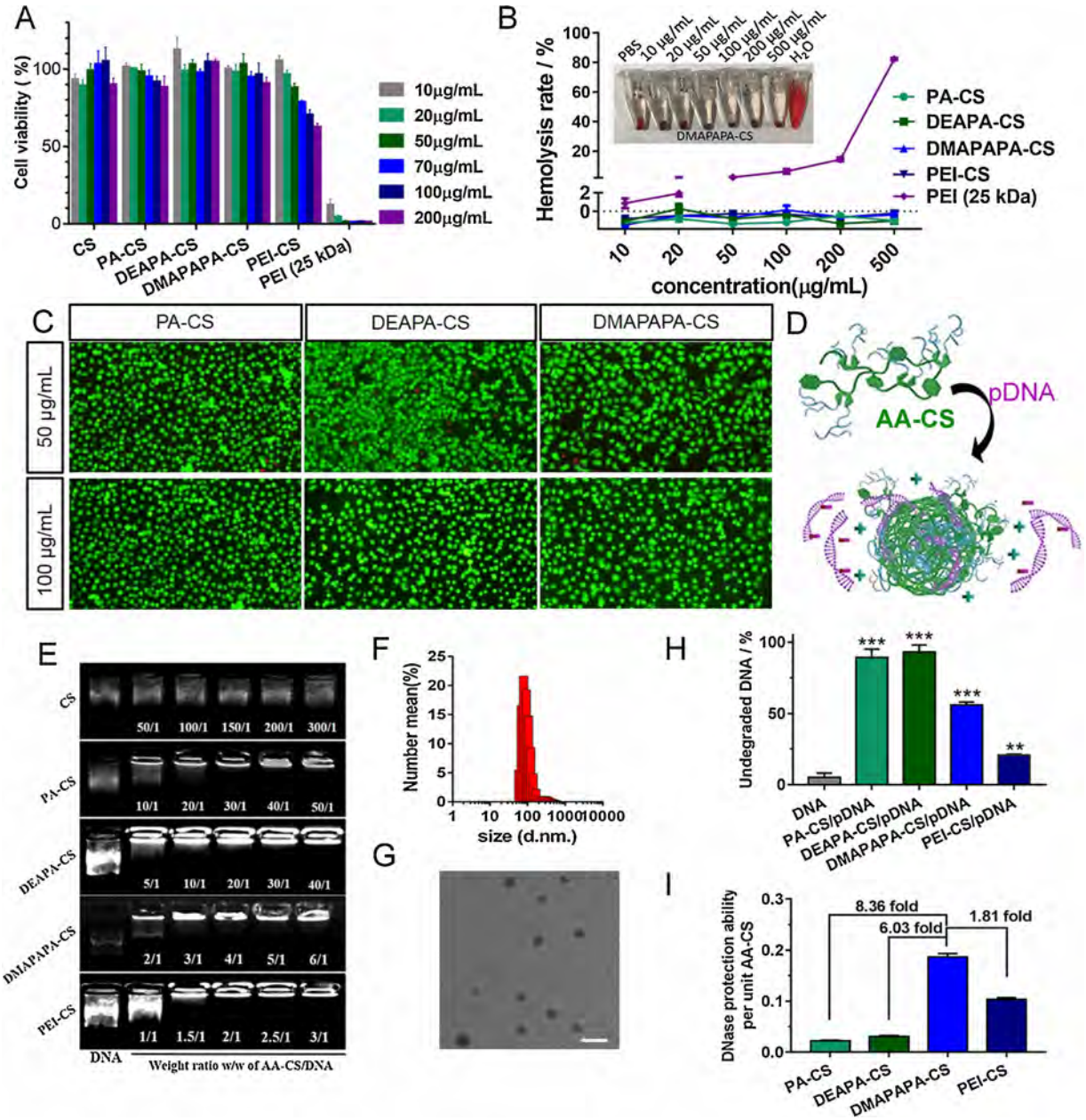


**Fig. 3.** Biocompatibility of alkylamine-chitosan and physicochemical characterization of the AA-CS/gene Complexes: (A) Cytotoxicity of chitosan and AA-CS polycations with different various concentrations in A549 cells from 10 to 200 μg/mL; (**B**) Blood hemolytic effects of AA-CS polycations. The red blood cells are treated with AA-CS polycations with various concentrations from 10 to 500 μg/mL. (**C**) Live and dead analysis of A549 cells in the different concentration of AA-CS; (**D**) Analogic structure of AA-CS which can form complexes with pDNA by electrostatic interactions between the positive amino groups and negative phosphate groups of pDNA. The AA-CS/pDNA complex is prepared by manual mixing of the AA-CS solution and pDNA solution; (**E**) Agarose gel electrophoresis of the AA-CS/pDNA (eGFP-$N_1$) complexes with different weight ratios (w/w); (**F**) Particle size distribution of the DMAPAPA-CS/DNA complexes in w/w ratio of 5/1; (**G**) TEM images of DMAPAPA-CS/pDNA with a weight ratio of 5/1 and the scale bars present 200 nm; (**H**) Undegraded DNA percentage of AA-CS/DNA complexes after DNase protection assay; (**I**) DNase protection ability of AA-CS calculated by undegraded DNA to AA-CS cost ratio.

In order to investigate the gene functionalization through AA-CS mediated transfection, p53 plasmid was employed to formulate the complexes with AA-CS and the functionalization of p53 was evaluated upon A549 cells. As shown in Fig. 4E and S19, AA-CS/p53 complexes could up-regulate the expression of p53 protein to varying degrees after 72 h transfection. In comparison, DMAPAPA-CS/p53 and PEI-CS/p53 complexes significantly increased the p53 protein expression, implying an efficient transfection. The nullification of p53 contributes to the survival and proliferation of cells, whereas the restoration of p53 could induce the cell cycle arrest and apoptosis (Komarov et al., 1999; Park, Park, & Na, 2015). To evaluate the functionalization of p53 through transfection, we next quantified the cell apoptosis by flow cytometry (Fig. 4F and S20). The A549 cells treated with PA-CS/p53, DEAPA-CS/p53, DMAPAPA-CS/p53, and PEI-CS/p53 complexes presented the percentages of apoptosis were 30.34 ± 1.63%, 23.27 ± 1.73%, 50.54 ± 2.90% and 41.67 ± 4.58%, respectively (Table S4). In accord with the p53 expression, DMAPAPA-CS/p53 treatment induced the highest apoptotic rate, which implied the most efficient delivery and functionalization of the loaded plasmid.

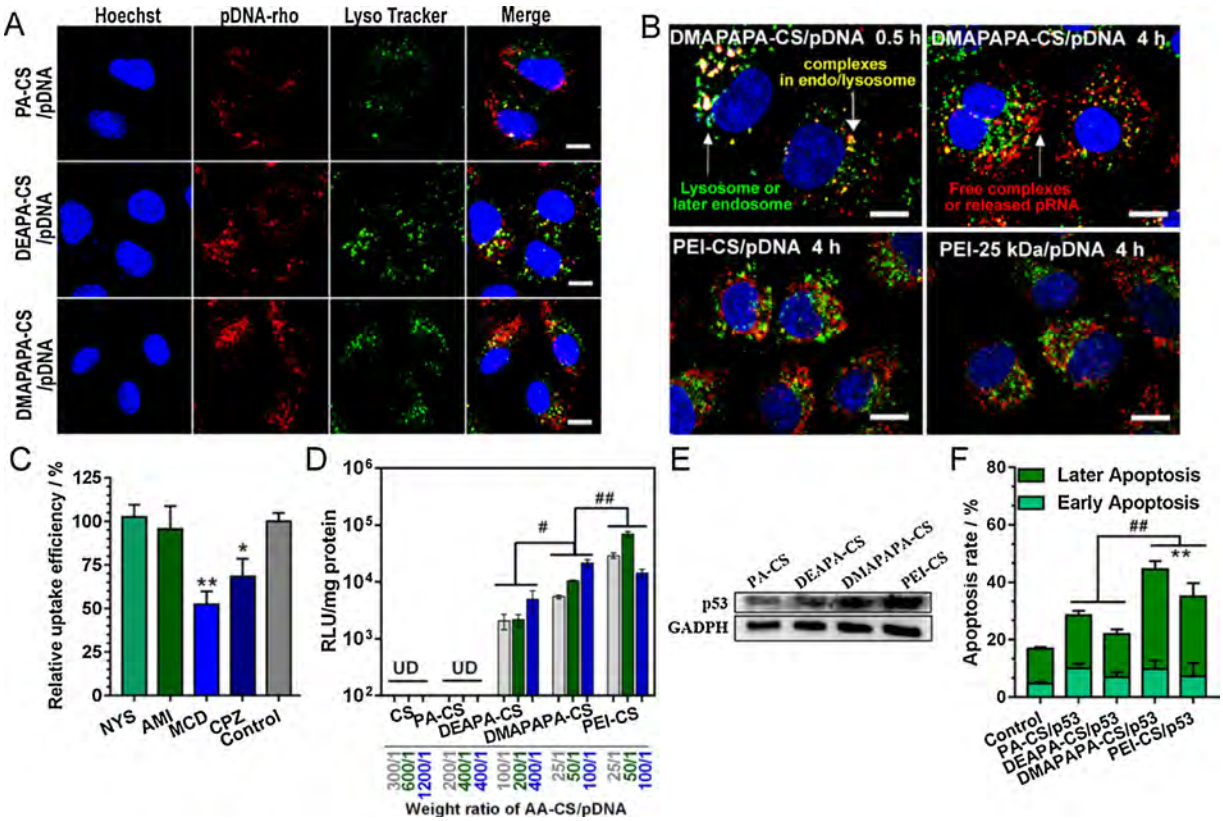


**Fig. 4.** Cellular uptake and endosomal escape of AA-CS/pDNA complexes: (A) CLSM images of the A549 cells after incubation with AA-CS/pDNA (2 μg/mL pDNA-rho) for 4 h. Hoechst 33342 (blue) and Lyso-Tracker Green are used to stain cell nuclei and lysosome respectively, the scale bar is 10 μm; (**B**) CLSM images of A549 cells after incubation with DMAPAPA-CS/pDNA-rho, PEI-CS/pDNA-rho, or PEI-25 kDa/pDNA-rho. The cells are stained with Lyso-Tracker Green and Hoechst 33342, the scale bar is 10 μm. (**C**) Investigation of cellular uptake mechanism. Relative uptake efficiency of DMAPAPA-CS/pDNA on A549 cells in the presence of various endocytosis inhibitors. Inhibitor of clathrin-mediated endocytosis: chlorpromazine (CPZ); inhibitor of lipid raft: methyl-β-cyclodextrin (MCD); inhibitor of macropinocytosis: amiloride (AMI); inhibitor of caveolinmediated endocytosis: nystatin (NYS). Transfection and p53 functionalization: (**D**) Transfection efficiency of A549 cells by the alkylamine-chitosan (AA-CS)/DNA (pGL4-control) complexes with various weight ratios (w/w). The transfection efficiency of the DMAPAPA-CS/DNA complexes is higher than that of the CS/DNA, PA-CS/DNA, and DEAPA-CS/DNA complexes ($p < 0.05$). (**E**) Western blot analysis of p53 protein expression at 72 h after transfection. (**F**) Flow cytometric analysis of apoptotic A549 cells at 72 h after treatments of complexes ($p < 0.01$).

### *3.7. Gene delivery in vivo and tumor inhibition on A549 xenograft model*

Base on the superior gene binding and *in vitro* transfection performance, DMAPAPA-CS was next tested as a gene carrier for *in vivo* tumor treatment. As illustrated in Fig. 5A, A549 solid tumor model was conducted in female BALB/c nude mice. We first investigated the tumor accumulation of DMAPAPA-CS/FITC-labeled siRNA (FAM-siRNA) via orthotopic injection. After 3 h post injection, the tumors were taken out surgically and examined by inverted fluorescence microscopy (Fig. 5A). In comparison, the CS/FAM-siRNA nanoparticles induced a barely scattered distribution of FITC signal in tumor tissues, while the fluorescence signal in the DMAPAPA-CS/FAM-siRNA group was observed at a wide range of tumor tissues (Fig. 5B). The statistical counting of FITC signal in equal-area sections indicated that the *in vivo* gene delivery efficiency of DMAPAPA-CS/FAM-siRNA was ~1.7 times higher than that of CS/FAM-siRNA. To further explore the permeability of DMAPAPA-CS/FAM-siRNA nanoparticles, we scanned the fluorescence signal in tumor sections from different depth. The observation (Fig. 5C) showed that the green fluorescence induced by CS/FAM-siRNA nanoparticles aggregated in the outer layer of tumors, while the fluorescence signal of DMAPAPA-CS/FAM-siRNA complexes was mostly dispersed at any scanned depth of the tumor tissues. The notable penetrability of DMAPAPA-CS could facilitate the subsequent gene therapy.

The A549 tumor-bearing mice were randomly divided into four groups, (I) PBS, (II) p53 plasmid, (III) CS/p53 and (IV) DMAPAPA-CS/p53 (Fig. 5D-G). Treatment was conducted via peritumoral injection at day 0, 3, and 6. The tumor inhibition in each treatment group was assessed by monitoring the tumor volume (Fig. 5E). Treatment with PBS or p53 plasmid showed little therapeutic effect against tumor progression, the tumor volume achieved 1000 ~ 1300 $mm^3$ at day 21. The CS/p53 manifested an inconspicuous inhibitory effect on tumor growth. After treatment, a rapid recurrence was observed. By contrast, a significant inhibition of tumor growth was realized in DMAPAPA-CS/p53 treatment group. The inhibitory rate reached to 59.0% as compared to that of control group. In addition, relatively low tumor weight confirmed the superior antitumor effect of DMAPAPA-CS/p53 (Fig. 5F). Taken together, these results demonstrated that the DMAPAPA-CS/p53 could exert a therapeutic potential against solid tumor owing to its enhanced tumor penetration and efficient *in vivo* transfection.

## 4. Conclusion

A series of AA-CS polycations were prepared by reconstructed pristine chitiosan with alkylamines (PA, DEAPA and DMAPAPA) to establish a new chitosan-based platform for gene delivery. The AA-CS, particularly, the DMAPAPA-CS, possessed strong binding capacity with pDNA (siRNA) and excellent biocompatibility. Importantly, the DMAPAPA-CS exhibited an improved buffering capacity that was derived from its secondary and tertiary amine groups with rational ratios. Boasting its buffering capacity, the DMAPAPA-CS/gene complexes overcame the intracellular barrier by promoting endo/lysosomal escape, leading to an enhanced transfection performance. *In vivo* studies

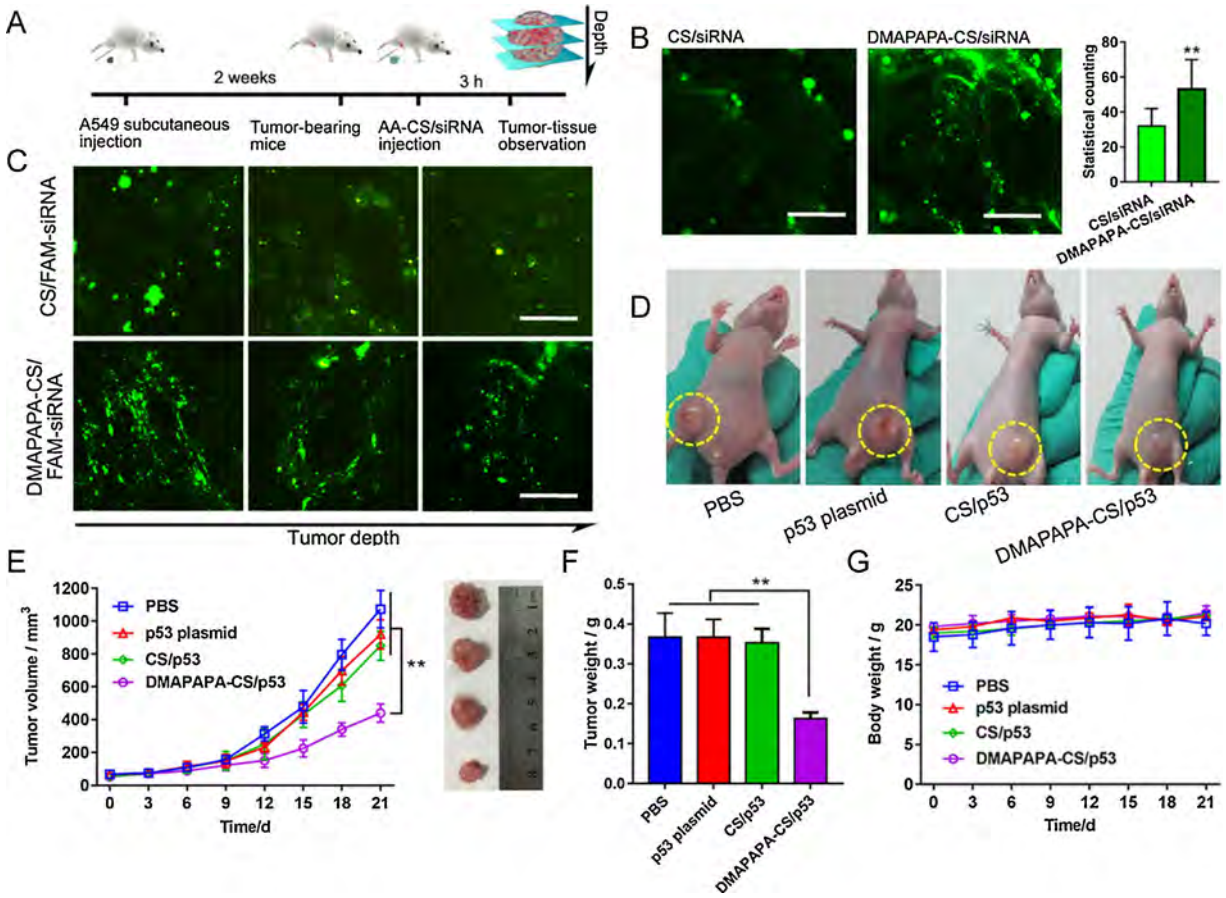


**Fig. 5.** Gene delivery and tumor inhibition *in vivo*. (**A**) Scheme of investigation of the delivery of AA-CS/RNA complex in tumor tissue; (**B**) Fluorescence images and statistical counting of green signal in tumor tissues, scale bar present 50 μm; (**C**) The fluorescence images of CS/FAM-siRNA, and DMAPAPA-CS/FAM-siRNA complexes biodistribution in tumor at different depth of tumor, 3 h after complexes were orthotopic injected into lung tumor bearing mice; (**D**) representative images of xenograft in mice and tumors; (**E**) tumor volumes and tumor pictures ; (**F**) weights of A549 xenografts; and (**G**) mouse weights during the assay.(** $P < 0.01$).

demonstrated that the DMAPAPA-CS/gene system with superior transfection behavior and tumorous penetrability exerted a therapeutic effect against solid tumor, manifesting a large potential as gene carriers in tumor therapy.

## Declaration of Competing Interest

There are no conflicts of interest to declare

## Acknowledgments

G. H, H. B., and G. T. designed the research. G. H., Q. C., W. W. and H. B. performed the research. G. H., J. W., and H. B. analyzed the data. P. C. contributed new reagents/analytic tools. G. H., H. B., and P. C. wrote the manuscript. This work was jointly supported by the National Natural Science Foundation of China (No. 51573161 & No. 81573003) and Hong Kong Research Grants Council (RGC) General Research Funds (GRF) Nos. CityU 11301215 and 11205617.

## Appendix A. Supplementary data

Supplementary material related to this article can be found, in the online version, at doi:https://doi.org/10.1016/j.carbpol.2019.115339.

## References

Bao, X., Wang, W., Wang, C., Wang, Y., Zhou, J., Ding, Y., et al. (2014). A chitosan-graft-PEI-candesartan conjugate for targeted co-delivery of drug and gene in anti-angiogenesis cancer therapy. *Biomaterials, 35*, 8450–8466. http://www.ncbi.nlm.nih.gov/pubmed/24997481.

Boussif, O., Lezoualc, F., Zanta, M. A., Mergny, M. D., Scherman, D., Demeneix, B., et al. (1995). A versatile vector for gene and oligonucleotide transfer into cells in culture and in vivo: Polyethylenimine. *Proceedings of the National Academy of Sciences, 92*, 7297. http://www.pnas.org/content/92/16/7297.abstract.

Byeon, J., Kim, H., Thompson, D., & Roberts, J. (2014). Aerosol-based fabrication of modified chitosans and their application for gene transfection. *ACS Applied Materials & Interfaces, 6*, 4597–4602. http://www.ncbi.nlm.nih.gov/pubmed/24628606.

Corsi, K., Chellat, F., Yahia, L., & Fernandes, J. (2003). Mesenchymal stem cells, MG63 and HEK293 transfection using chitosan-DNA nanoparticles. *Biomaterials, 24*, 1255–1264. http://www.sciencedirect.com/science/article/pii/S0142961202005070.

Edson, J. A., Ingato, D., Wu, S., Lee, B., & Kwon, Y. J. (2018). Aqueous-soluble, acid-transforming chitosan for efficient and stimuli-responsive gene silencing. *Biomacromolecules, 19*, 1508–1516. https://doi.org/10.1021/acs.biomac.8b00170.

Han, L., Tang, C., & Yin, C. (2015). Dual-targeting and pH/redox-responsive multi-layered nanocomplexes for smart co-delivery of doxorubicin and siRNA. *Biomaterials, 60*, 42–52. http://www.ncbi.nlm.nih.gov/pubmed/25982552.

Hu, Q., Sun, W., Qian, C., Wang, C., Bomba, H. N., & Gu, Z. (2015). Anticancer platelet-mimicking nanovehicles. *Advanced Materials, 27*, 7043–7050. https://www.ncbi.nlm.nih.gov/pubmed/26416431.

Jiang, Q. Y., Lai, L. H., Shen, J., Wang, Q. Q., Xu, F. J., & Tang, G. P. (2011). Gene delivery to tumor cells by cationic polymeric nanovectors coupled to folic acid and the cell-penetrating peptide octaarginine. *Biomaterials, 32*, 7253–7262. https://www.ncbi.nlm.nih.gov/pubmed/21715001.

Jiang, H., Kim, Y., Arote, R., Nah, J., Cho, M., Choi, Y., et al. (2007). Chitosan-graft-polyethylenimine as a gene carrier. *Journal of Controlled Release : Official Journal of the Controlled Release Society, 117*, 273–280. http://www.ncbi.nlm.nih.gov/pubmed/17166614.

Jiang, H. L., Kwon, J. T., Kim, Y. K., Kim, E. M., Arote, R., Jeong, H. J., et al. (2007). Galactosylated chitosan-graft-polyethylenimine as a gene carrier for hepatocyte targeting. *Gene Therapy, 14*, 1389. https://doi.org/10.1038/sj.gt.3302997.

Kiang, T., Bright, C., Cheung, C., Stayton, P., Hoffman, A., & Leong, K. (2004). Formulation of chitosan-DNA nanoparticles with poly(propyl acrylic acid) enhances gene expression. *Journal of Biomaterials Science Polymer Edition, 15*, 1405–1421. https://doi.org/10.1163/1568562042368112.

Kim, T., Kim, S., Akaike, T., & Cho, C. (2005). Synergistic effect of poly(ethylenimine) on

the transfection efficiency of galactosylated chitosan/DNA complexes. *Journal of Controlled Release : Official Journal of the Controlled Release Society, 105*, 354–366. http://www.ncbi.nlm.nih.gov/pubmed/15949861.

Komarov, P. G., Komarova, E. A., Kondratov, R. V., Christov-Tselkov, K., Coon, J. S., Chernov, M. V., et al. (1999). A chemical inhibitor of p53 that protects mice from the side effects of Cancer therapy. *Science, 285*, 1733. http://science.sciencemag.org/content/285/5434/1733.abstract.

Lai, W., & Wong, W. (2018). Design of polymeric gene carriers for effective intracellular delivery. *Trends in Biotechnology, 36*, 713–728. http://www.ncbi.nlm.nih.gov/pubmed/29525137.

Li, C., Guo, T., Zhou, D., Hu, Y., Zhou, H., Wang, S., et al. (2011). A novel glutathione modified chitosan conjugate for efficient gene delivery. *Journal of Controlled Release : Official Journal of the Controlled Release Society, 154*, 177–188. http://www.ncbi.nlm.nih.gov/pubmed/21689698.

Liu, X., Howard, K., Dong, M., Andersen, M., Rahbek, U., Johnsen, M., et al. (2007). The influence of polymeric properties on chitosan/siRNA nanoparticle formulation and gene silencing. *Biomaterials, 28*, 1280–1288. http://www.ncbi.nlm.nih.gov/pubmed/17126901.

Liu, X., Wu, M., Hu, Q., Bai, H., Zhang, S., Shen, Y., et al. (2016). Redox-activated light-up nanomicelle for precise imaging-guided Cancer therapy and real-time pharmacokinetic monitoring. *ACS Nano, 10*, 11385–11396. https://doi.org/10.1021/acsnano.6b06688.

Mao, S., Sun, W., & Kissel, T. (2010). Chitosan-based formulations for delivery of DNA and siRNA. *Advanced Drug Delivery Reviews, 62*, 12–27. http://www.sciencedirect.com/science/article/pii/S0169409X09002816.

Martins, G. O., Segalla Petronio, M., Furuyama Lima, A. M., Martinez Junior, A. M., de Oliveira Tiera, V. A., de Freitas Calmon, M., et al. (2019). Amphipathic chitosans improve the physicochemical properties of siRNA-chitosan nanoparticles at physiological conditions. *Carbohydrate Polymers, 216*, 332–342. https://www.ncbi.nlm.nih.gov/pubmed/31047074.

Müller, C., Rahmat, D., Sarti, F., Leithner, K., & Bernkop-Schnürch, A. (2012). Immobilization of 2-mercaptoethylamine on oxidized chitosan: A substantially mucoadhesive and permeation enhancing polymer. *Journal of Materials Chemistry, 22*, 3899–3908. https://doi.org/10.1039/C2JM15164B.

Nam, J., & Nah, J. (2016). Target gene delivery from targeting ligand conjugated chitosan–PEI copolymer for cancer therapy. *Carbohydrate Polymers, 135*, 153–161. http://www.sciencedirect.com/science/article/pii/S0144861715007948.

Nielsen, C. (1998). Sequences lead to tree of worms. *Nature, 392*, 25. https://doi.org/10.1038/32058.

Park, S., Park, W., & Na, K. (2015). Tumor intracellular-environment responsive materials shielded nano-complexes for highly efficient light-triggered gene delivery without cargo gene damage. *Advanced Functional Materials, 25*, 3472–3482. https://doi.org/10.1002/adfm.201500737.

Ragelle, H., Vandermeulen, G., & Préat, V. (2013). Chitosan-based siRNA delivery systems. *Journal of Controlled Release : Official Journal of the Controlled Release Society, 172*, 207–218. http://www.sciencedirect.com/science/article/pii/S0168365913004628.

Rahimi, M., Safa, K. D., & Salehi, R. (2017). Co-delivery of doxorubicin and methotrexate by dendritic chitosan-g-mPEG as a magnetic nanocarrier for multi-drug delivery in combination chemotherapy. *Polymer Chemistry, 8*, 7333–7350. https://doi.org/10.1039/C7PY01701D.

Richardson, S. W., Kolbe, H. J., & Duncan, R. (1999). Potential of low molecular mass chitosan as a DNA delivery system: Biocompatibility, body distribution and ability to complex and protect DNA. *International Journal of Pharmaceutics, 178*, 231–243. http://www.sciencedirect.com/science/article/pii/S0378517398003780.

Rudzinski, W., & Aminabhavi, T. (2010). Chitosan as a carrier for targeted delivery of small interfering RNA. *International Journal of Pharmaceutics, 399*, 1–11. http://www.ncbi.nlm.nih.gov/pubmed/20732398.

Sahoo, A. K., Banerjee, S., Ghosh, S. S., & Chattopadhyay, A. (2014). Simultaneous RGB emitting Au nanoclusters in chitosan nanoparticles for anticancer gene theranostics. *ACS Applied Materials & Interfaces, 6*, 712–724. http://www.ncbi.nlm.nih.gov/pubmed/24281656.

Schroedter, A., & Weller, H. (2002). Ligand design and bioconjugation of colloidal gold nanoparticles. *Angewandte Chemie International Edition, 41*, 3218–3221. https://doi.org/10.1002/1521-3773(20020902)41:17<3218::AID-ANIE3218>3.0.CO;2-P.

Shen, J., Zhao, D., Li, W., Hu, Q., Wang, Q., Xu, F., et al. (2013). A polyethylenimine-mimetic biodegradable polycation gene vector and the effect of amine composition in transfection efficiency. *Biomaterials, 34*, 4520–4531. http://www.sciencedirect.com/science/article/pii/S0142961213002664.

Shi, L., Tang, G. P., Gao, S. J., Ma, Y. X., Liu, B. H., Li, Y., et al. (2003). Repeated intrathecal administration of plasmid DNA complexed with polyethylene glycol-grafted polyethylenimine led to prolonged transgene expression in the spinal cord. *Gene Therapy, 10*, 1179. https://doi.org/10.1038/sj.gt.3301970.

Sirvio, J., Hyvakko, U., Liimatainen, H., Niinimaki, J., & Hormi, O. (2011). Periodate oxidation of cellulose at elevated temperatures using metal salts as cellulose activators. *Carbohydrate Polymers, 83*, 1293–1297. http://www.sciencedirect.com/science/article/pii/S0144861710007691.

Sonawane, N. D., Szoka, F. C., Jr, & Verkman, A. S. (2003). Chloride accumulation and swelling in endosomes enhances DNA transfer by polyamine-DNA polyplexes. *The Journal of Biological Chemistry, 278*, 44826–44831. https://www.ncbi.nlm.nih.gov/pubmed/12944394.

Verma, I., & Somia, N. (1997). Gene therapy - promises, problems and prospects. *Nature, 389*, 239. https://doi.org/10.1038/38410.

Vold, I., & Christensen, B. (2005). Periodate oxidation of chitosans with different chemical compositions. *Carbohydrate Research, 340*, 679–684. http://www.ncbi.nlm.nih.gov/pubmed/15721340.

Wu, M., Liu, X., Jin, W., Li, Y., Li, Y., Hu, Q., et al. (2017). Targeting ETS1 with RNAi-based supramolecular nanoassemblies for multidrug-resistant breast cancer therapy. *Journal of Controlled Release : Official Journal of the Controlled Release Society, 253*, 110–121. https://www.ncbi.nlm.nih.gov/pubmed/28302581.

Yang, C., Gao, S., Dagnaes-Hansen, F., Jakobsen, M., & Kjems, J. (2017). Impact of PEG chain length on the physical properties and bioactivity of PEGylated Chitosan/siRNA nanoparticles in vitro and in vivo. *ACS Applied Materials & Interfaces, 9*, 12203–12216. http://www.ncbi.nlm.nih.gov/pubmed/28332829.

# Supporting Information

# Reconstructed Chitosan with Alkylamine for Enhanced Gene Delivery by Promoting Endosomal Escape

***Guojun Huang [a, b], Qi Chen [a, b], Wangteng Wu [a, c], Jianwei Wang [a], Paul K Chu [b], Hongzhen Bai [a]*, Guping Tang [a, b]****

*a. Department of Chemistry, Zhejiang University, Hangzhou 310028, China*

*b. Department of Physics and Department of Materials Science and Engineering, City University of Hong Kong, Tat Chee Avenue, Kowloon, Hong Kong, China*

*c. School of Medicine, Zhejiang University, Hangzhou 310019, China*

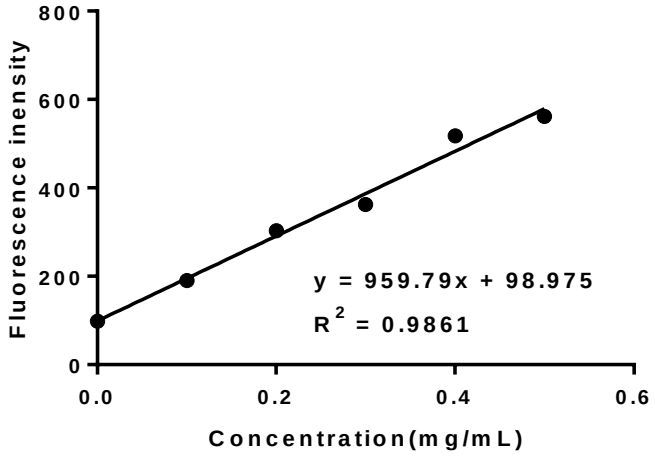


Fig. S1. Standard curve of fluorescamine assay on chitosan oligosaccharide.

Table S1. The degree of oxidized CS in OCS

| Sample | Reaction conditions | Determined by $^1$H NMR (mol%) | Determined by fluorescamine assay (mol%) |
|---|---|---|---|
| OCS-1 | 75 mM $NaIO_4$, RT*, 2h, light proof, sodium acetate buffer (pH 4.0) | 16 | 19.1 |
| OCS-2 | 75 mM $NaIO_4$, RT, 4h, light proof, sodium acetate buffer (pH 4.0) | 38 | 40.4 |
| OCS-3 | 75 mM $NaIO_4$, 60℃, 4h, light proof, sodium acetate buffer (pH 4.0) | 54 | 57.1 |

*: RT= room temperature.

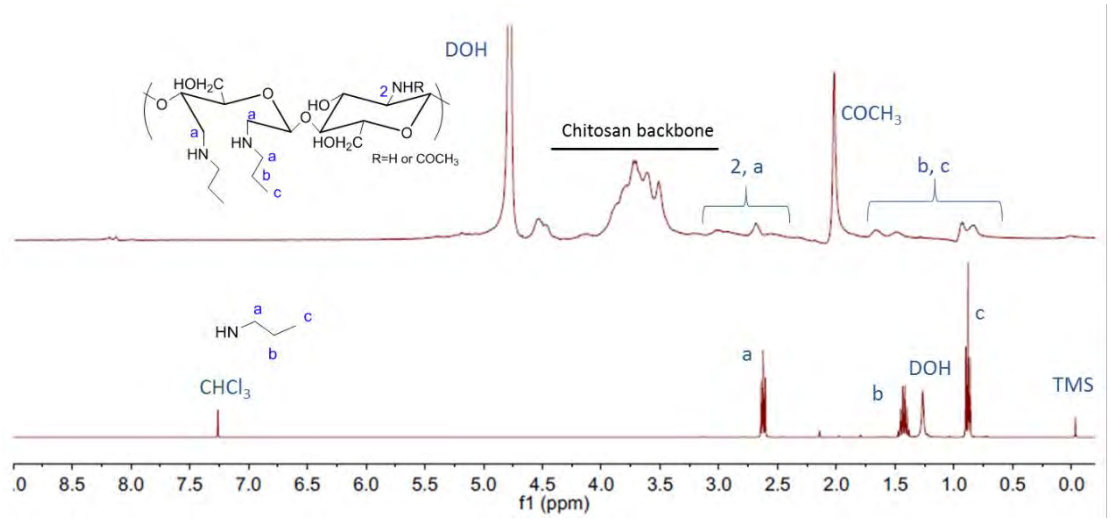


Fig. S2. $^1$H NMR spectrum of PA-CS in $D_2O$ and PA in $CDCl_3$.

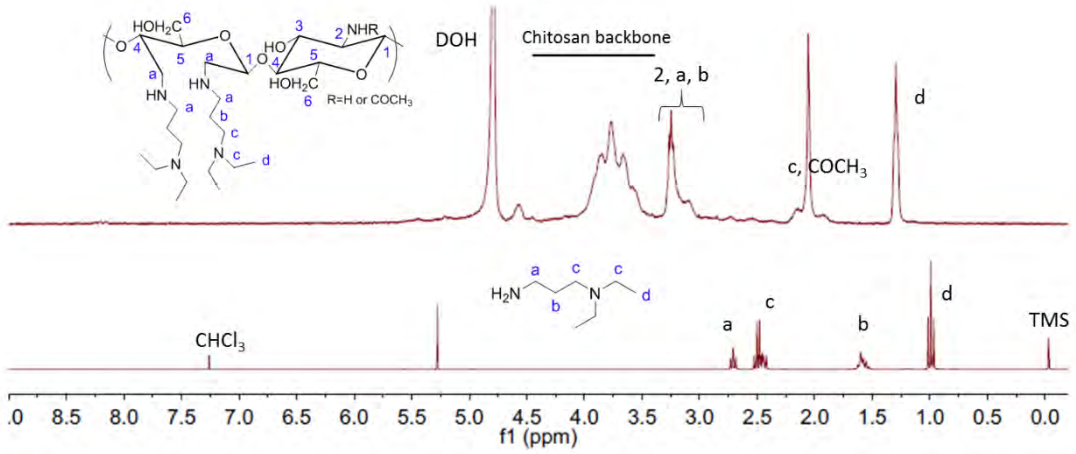


Fig. S3. $^{1}H$ NMR spectrum of DEAPA-CS in $D_2O$ and DEAPA in $CDCl_3$.

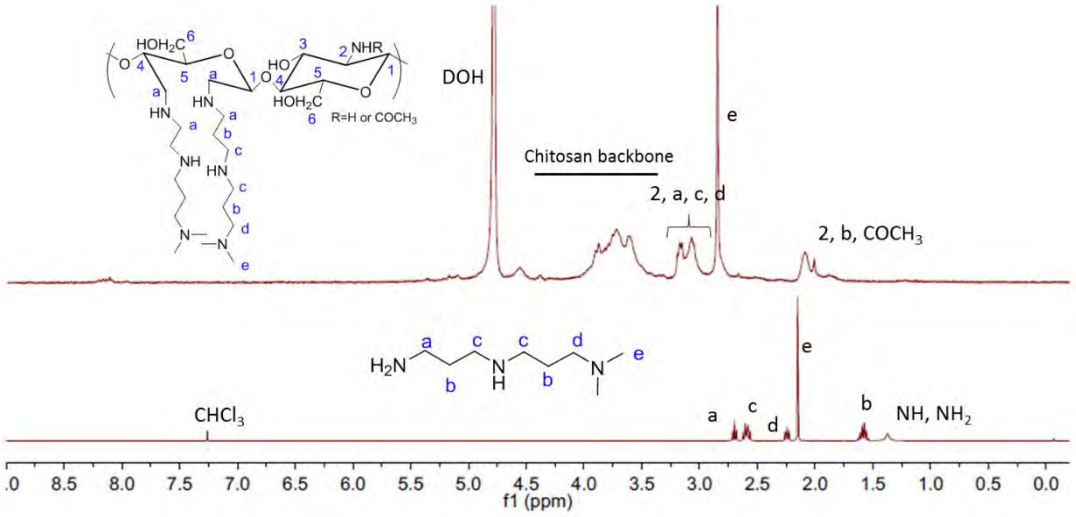


Fig. S4.$^{1}H$ NMR spectrum of DMAPAPA-CS in $D_2O$ and DMAPAPA in $CDCl_3$.

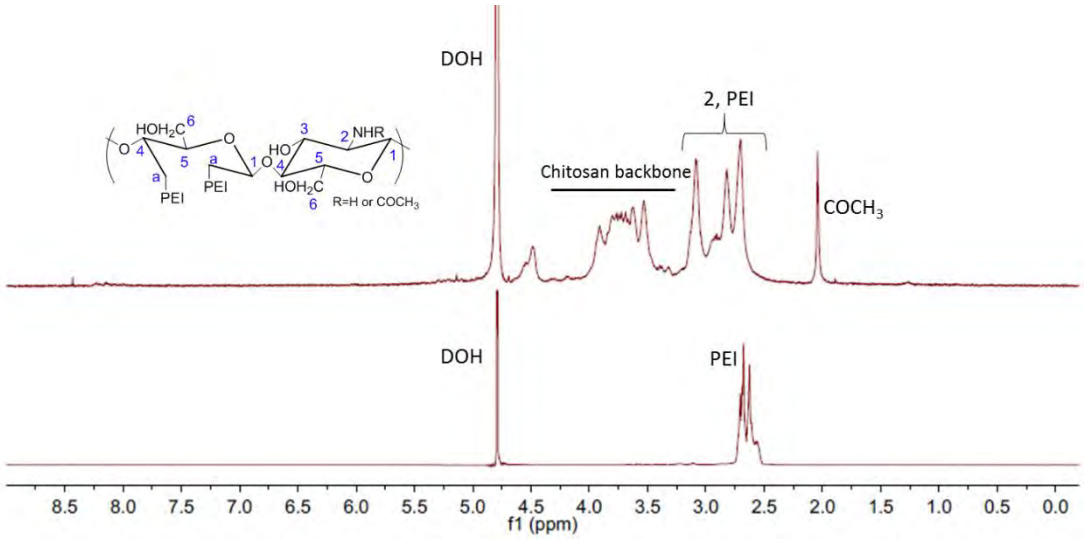

Fig. S5.$^{1}$H NMR spectrum of PEI-CS and PEI-600 in $D_2O$.

Table S2. The degree of amino compounds conjugated chitosan in AA-CS determined by$^{1}$H NMR and fluorescamine assay

| Sample | Determined by $^{1}$H NMR(mol%) | Determined by fluorescamine assay(mol%)[a] |
|---|---|---|
| PA-CS | 22.00 | 25.2 |
| DEAPA-CS | 22.67 | 21.0 |
| DMAPAPA-CS | 20.17 | 22.9 |
| PEI-CS | 15.71 | -[b] |

a, Approximation. Because we hypothesize that D.D. of chitosan wsa not changed after grafted with alkylamines;

b, Mass fraction of chitosan in PEI-CS can not determined by fluorescamine assay.

Table S3. Molecular weight determined by GPC.

| Sample* | Mn/Da | Mw/Da | Mw/Mn |
|---|---|---|---|
| PA-CS | 7 356 | 8 004 | 1.088 |
| DEAPA-CS | 6 714 | 8 407 | 1.252 |
| DMAPAPA-CS | 8 777 | 9 786 | 1.115 |
| PEI-CS | 7 272 | 9 076 | 1.248 |

* Chitosan (MW: 100-300 kDa, degree of deacetylation ⩾ 90%) was purchased from J&K Chemical Ltd.. After periodate oxidation, the molecular weight of chitosan was 7-10 kDa. Commercially available chitosan oligosaccharide was used for calibration.

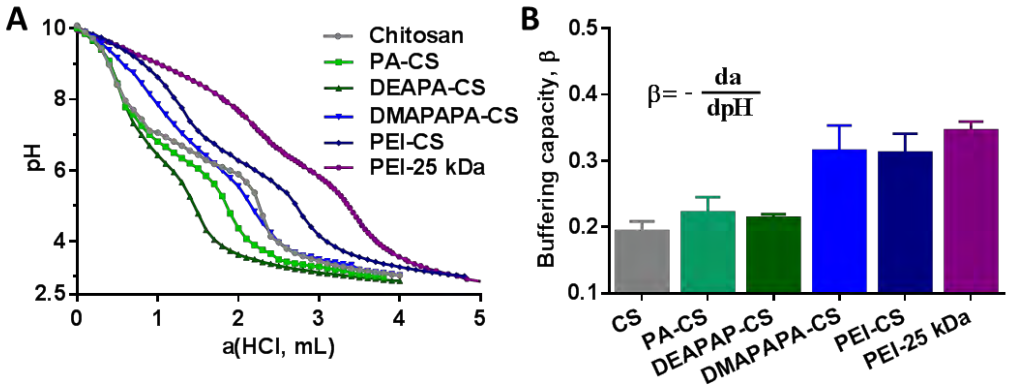


Fig. S6. A) Acid-base titration profiles of AA-CS by HCl in 150 mM NaCl solution; B) the value of -da/dpH in the two peaks of first-order derivative curve.

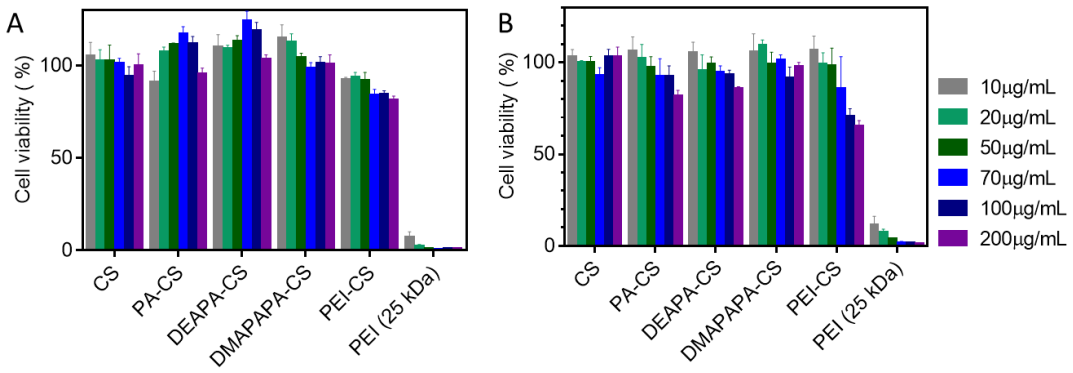


Fig. S7. Cytotoxicity of chitosan and AA-CS polymers and PEI (25 kDa) with different various concentrations in (A) MCF-7 cells and (B) HEK293 cells from 10 to 200 μg/mL.

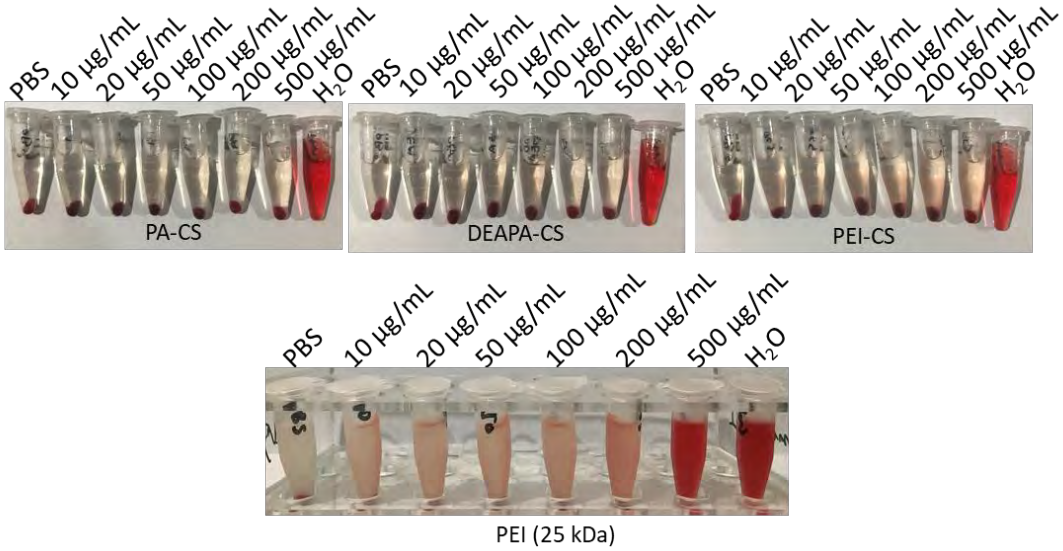


Fig. S8. Pictures of RBCs treated with PA-CS, DEAPA-CS, PEI-CS, and PEI (25 kDa) of different concentration, as compared to the water and PBS groups.

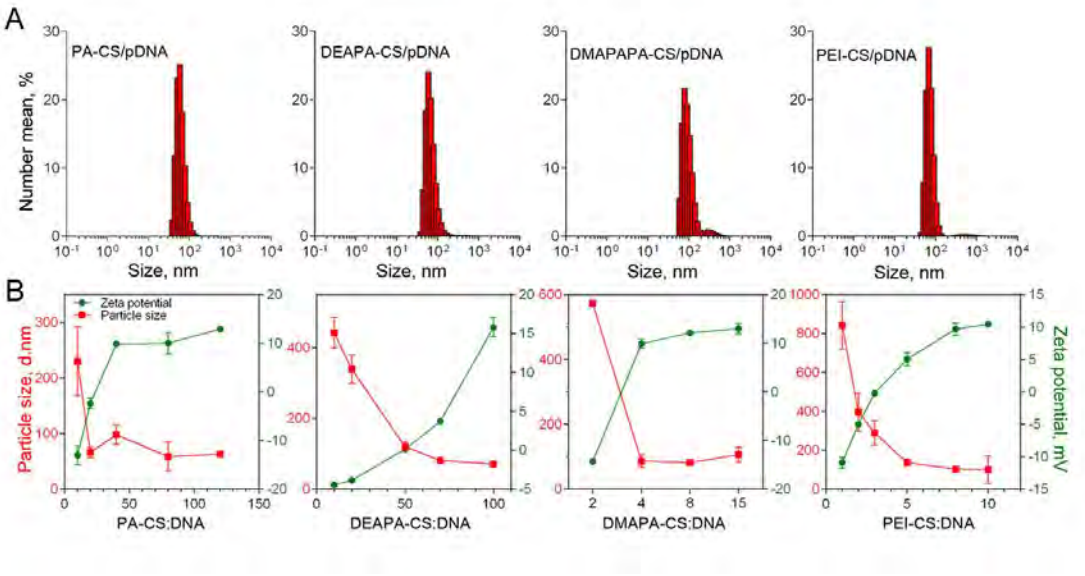


Fig. S9. (A) Particle size distribution of the PA-CS/DNA, DEAPA-CS/DNA, DMAPAPA-CS/DNA, and PEI-CS/DNA complexes with w/w ratios of 40, 20, 5, and 3, respectively; (B) Particle size and zeta potential of the PA-CS/DNA, DEAPA-CS/DNA, and PEI-CS/DNA complexes with different weight ratios;

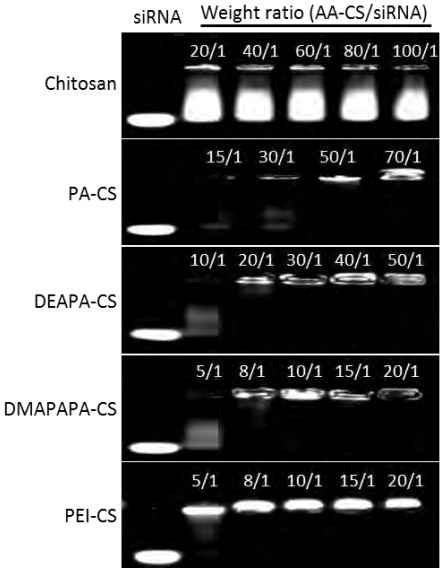


Fig. S10. Agarose gel electrophoresis of Alkylamine-Chitosan (AA-CS)/siRNA (siGFP) complexes at various weight ratios (w/w).

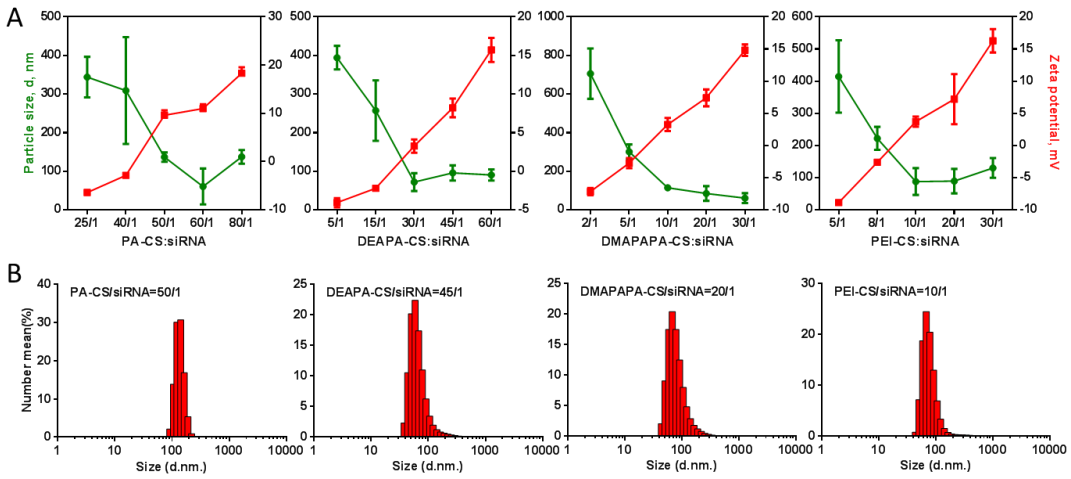


Fig. S11. A) Particle size and Zeta potential of PA-CS/siRNA, DEAPA-CS/siRNA, DMAPAPA-CS/siRNA, and PEI-CS/siRNA complexes at various weight ratios. B) Particle size distribution PA-CS/siRNA, DEAPA-CS/siRNA, DMAPAPA-CS/siRNA, and PEI-CS/siRNA complexes at w/w ratio of 40, 20, 5, and 3, respectively.

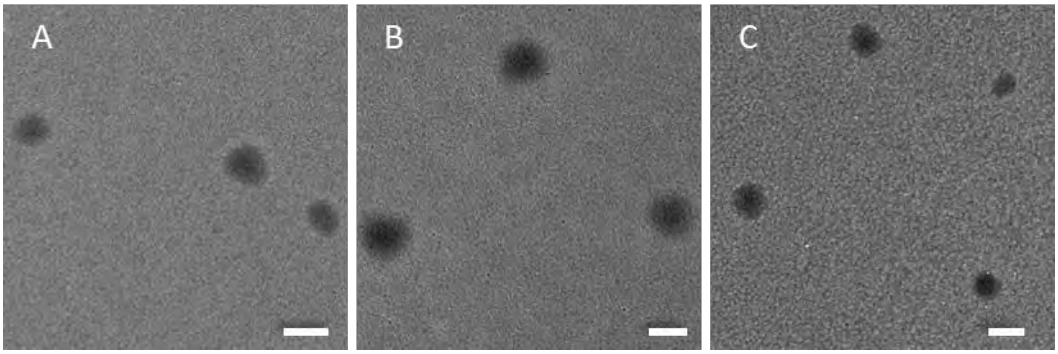


Fig. S12. TEM images of A) PA-CS/DNA, B) DEAPA-CS/DNA, C) PEI-CS/DNA complexes at w/w ratio of 40, 20, and 3, respectively. The scale bar present 100nm.

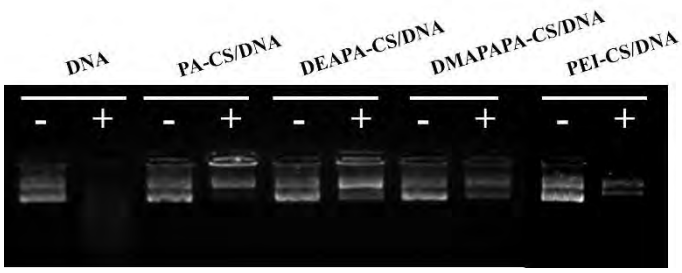


Fig. S13. Agarose gel electrophoresis image of the DNase protection assay. DNA is released by adding 5 mg/mL heparin to the PA-CS/DNA, DEAPA-CS/DNA, DMAPAPA-CS/DNA, and PEI-CS/DNA complexes with weight ratios of 40, 20, 5 and 3, respectively.

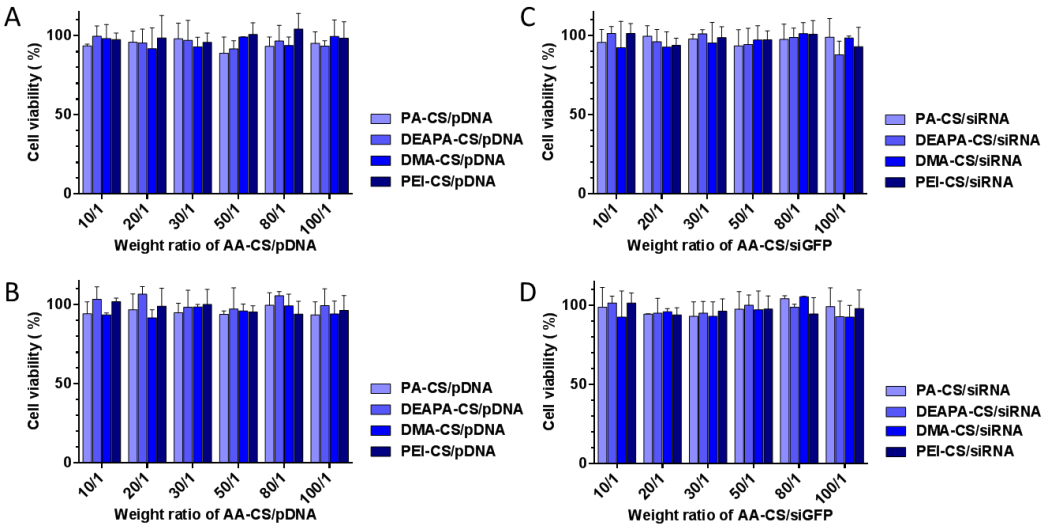


Fig. S14. Cytotoxicity of AA-CS/pDNA(pGL-4) complexes at different various weight ratio in (A) HEK293 cells and (B) A549 cells from 10/1 to 100/1, Cytotoxicity of AA-CS/siGFP complexes at different various weight ratio in (C) HEK293 cells and (D) A549 cells from 10/1 to 100/1;

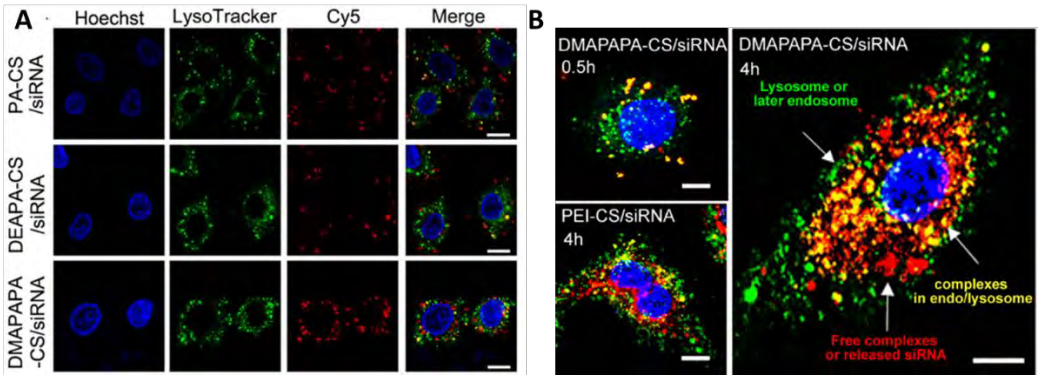


Fig. S15. (**A**) CLSM images of the A549 cells after incubation with AA-CS/siRNA (2 μg/mL Cy5-siRNA) for 4 h.; (**B**) Z-stack CLSM images of A549 cells after incubation with DMAPAPA-CS/Cy5-siRNA or PEI-CS/Cy5-siRNA. Hoechst 33342 (blue) and Lyso-Tracker Green are used to stain cell nuclei and lysosome respectively, the scale bar is 10 μm.

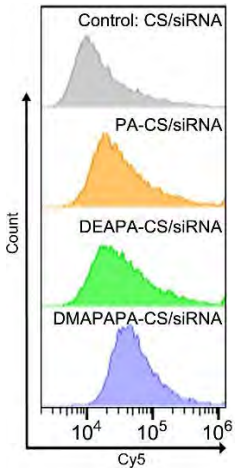


Fig. S16. Flow cytometry analysis of Cy5 in the A549 cells incubated with chitosan/Cy5-siRNA and AA-CS/Cy5-siRNA.

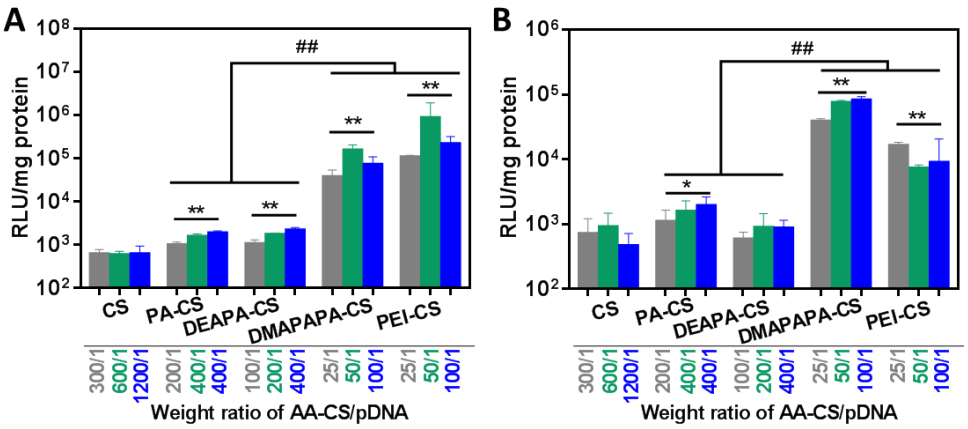


Fig. S17. Transfection efficiency of (A) HEK293 and (B) MCF-7 cells by the alkylamine-chitosan (AA-CS)/DNA (pGL4-control) complexes with various weight ratios (w/w).

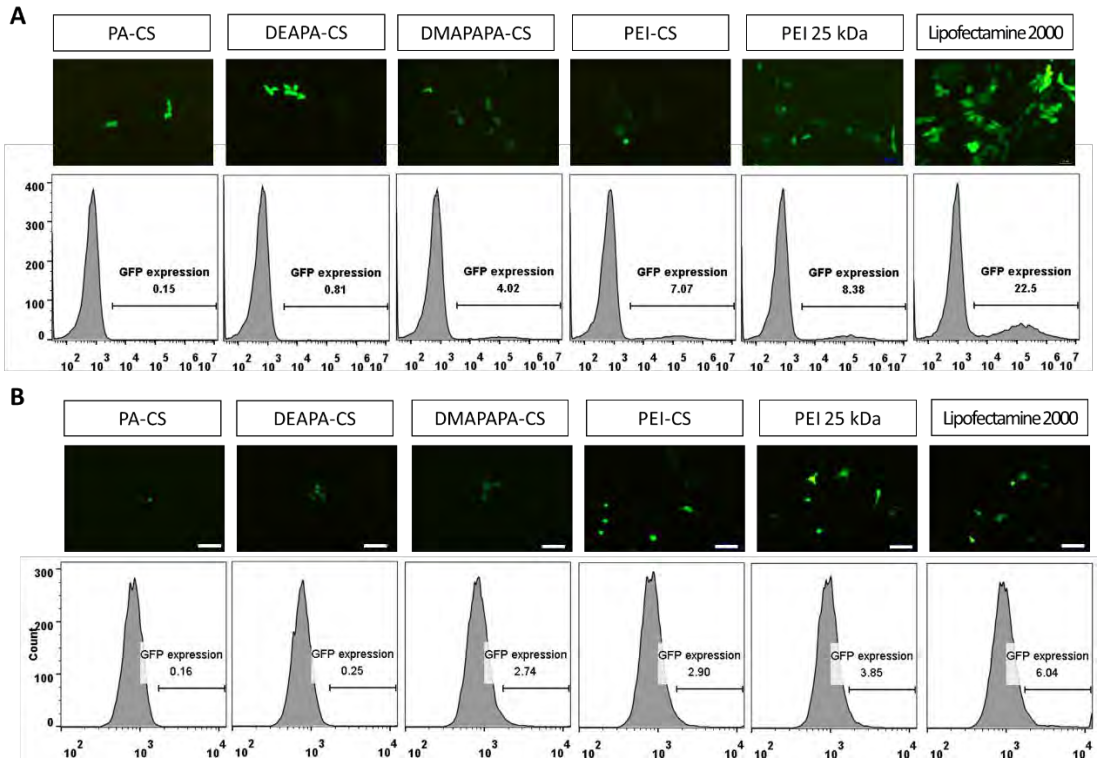


Fig. S18. GFP transfection carried out in (A) HEK293 and (B) A549 cells mediated by the AA-CS, PEI-CS, PEI 25 kDa, and Lipofectamine 2000.

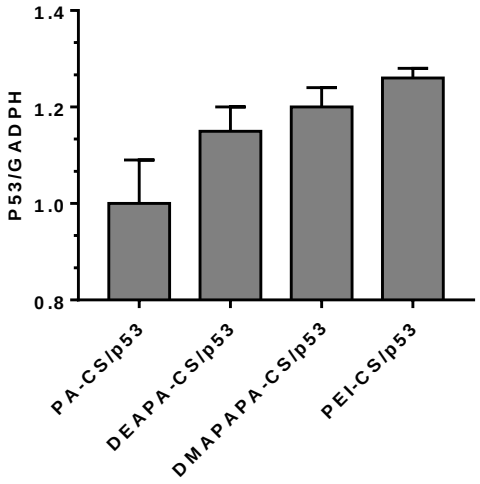


Fig. S19. Analysis of light intensities of p53 protein expression from Western blot results.

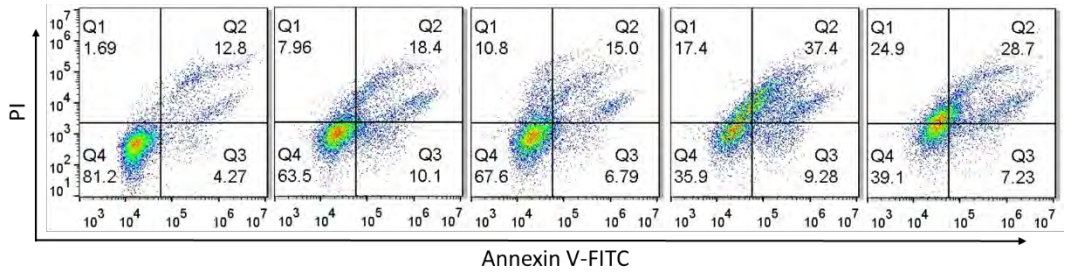


Fig. S20. Flow cytometric analysis of apoptotic A549 cells

Table S4. The percentages of apoptotic A549 cells after treatment.

| Sample | Apoptosis rate / % |
|---|---|
| Control | 17.56± 0.63 |
| PA-CS/p53 | 29.37± 1.53 |
| DEAPA-CS/p53 | 22.38± 1.50 |
| DMAPAPA-CS/p53 | 48.63± 2.94 |
| PEI-CS/p53 | 38.79± 4.56 |